Morpho-functional characterisation of cœlomocytes in the aquacultivated sea cucumber *Holothuria scabra*: from cell diversity to transcriptomic immune response

Noé Wambreuse[1,2], Guillaume Caulier[1,2], Igor Eeckhaut[1,2], Laura Borrello[1], Fabrice Bureau[3], Laurence Fievez[3], Jérôme Delroisse[1,3]

[1] Biology of Marine Organisms and Biomimetics Unit, Research Institute for Biosciences, University of Mons (UMONS), 7000 Mons, Belgium

[2] Belaza Marine Station (IH.SM-UMONS-ULB-ULIEGE), Toliara 601, Madagascar

[3] Laboratory of Cellular and Molecular Immunology, GIGA Research, University of Liège, 4000 Liège, Belgium

* Corresponding author. Email: Noe.Wambreuse@umons.ac.be. Postal address: 6, Avenue du Champ de Mars, 7000 Mons, Belgium

Keywords: Echinodermata, Immune cells, Immune genes, Humoral response, Cellular response, Lipopolysaccharide, Transcriptomics, RNA-sequencing

Graphical abstract

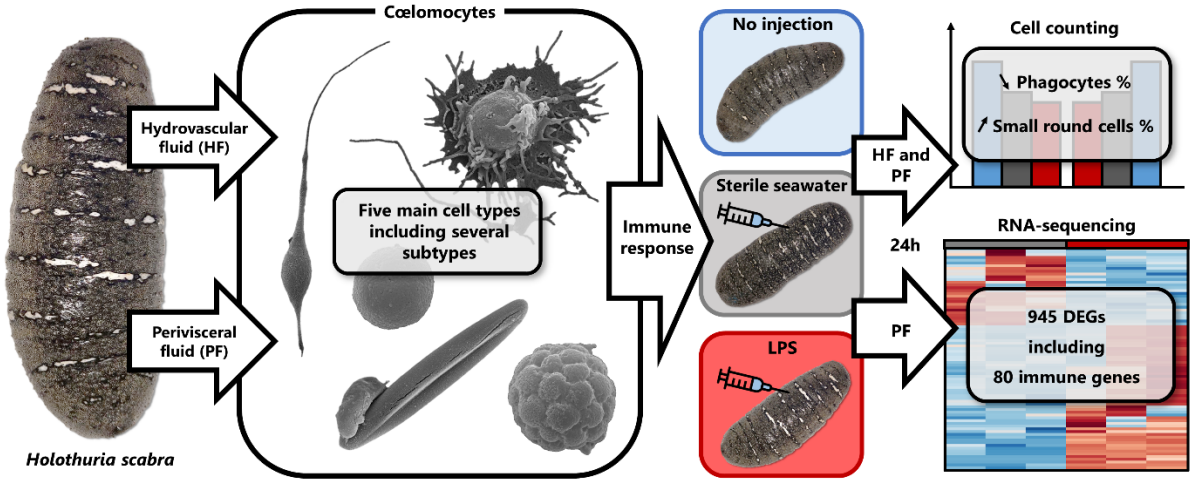

Abstract

Holothuria scabra is one of the most valuable species of sea cucumber owing to its exploitation as a seafood product. This study aims to describe the main molecular and cellular actors in the immunology of the holothuroid *H. scabra*. First, a detailed description of the immune cells – the cœlomocytes – is provided, highlighting five main cell types including phagocytes, small round cells (SRCs), spherulocytes, fusiform cells, and crystal cells, with a further five subtypes identified using transmission electron microscopy. Cœlomocyte aggregates were also described morphologically, yielding two main types, one comprising three successive maturation stages. A comparison of the concentration and proportion of cell populations was carried out between the two main body fluids, namely the hydrovascular fluid of the Polian vesicle (HF) and the perivisceral fluid of the general cavity (PF), and no clear relation could be revealed. Next, the cœlomocyte immune response was studied 24 hours after lipopolysaccharide (LPS) injection in the two body fluids. Firstly, the fluctuation in cell populations was assessed, and despite a high inter-individual variability, it shows a decrease in the phagocyte proportion and an increase in the SRC proportion.

Secondly, the differential gene expression of PF cœlomocytes was studied by *de novo* RNA-sequencing between LPS-injected and control-injected individuals: 945 genes were differentially expressed, including 673 up-regulated and 272 down-regulated in the LPS-injected individuals. Among these genes, 80 had a presumed function in immunity based on their annotation, covering a wide range of immune mechanisms. Overall, this study reveals a complex immune system at both molecular and cellular levels and constitutes a baseline reference on *H. scabra* immunity, which may be useful for the development of sustainable aquaculture and provides valuable data for comparative immunology.

1. Introduction

Sea cucumbers (*i.e.* holothuroids) are benthic marine invertebrates belonging to the phylum Echinodermata. Some species are crucial for marine ecosystems by acting as keystone bioturbators and around 70 species also have a high economic value owing to their exploitation in Asian gastronomy and traditional pharmacopoeia [1]. *Holothuria scabra*, a tropical sea cucumber living in the shallow seabed of Indo-Pacific waters, is among the most prized species [2]. In recent decades, its overexploitation has led to significant declines in wild stocks [1,2]. While conservation actions and the emergence of sustainable aquacultures offer good hopes for the future of this endangered species, *H. scabra* is subjected to epidemic diseases that lead to significant mortalities, both in the wild and in aquaculture facilities [2,3]. To better understand the development of these diseases in this species, and more broadly in sea cucumbers, it is necessary to gain knowledge about their immune system that remains understudied.

The immunity of echinoderms is mediated by free-circulating cells, the cœlomocytes, that are involved in numerous functions including phagocytosis, encapsulation, and

64 wound healing [4]. These particular cells can be found in a wide variety of tissues but
65 are particularly abundant within the perivisceral fluid from the general cavity (PF) and
66 the hydrovascular fluid from the water vascular system (HF). In the last decades,
67 numerous studies have described various cœlomocyte types in different species using
68 a large variety of methods (*e.g.* [5–7]). Although some cell types are common to
69 different species, many different designations exist in the literature which complicate
70 the establishment of a generalised coelomocyte classification. The most accepted
71 ones comprise six to seven cell types including phagocytes, spherulocytes, vibratile
72 cells, hemocytes, progenitor cells, crystal cells and fusiform cells [4,8]. In *H. scabra*,
73 little information exists about cœlomocytes and, to our knowledge, only Prompoon et
74 al. [9] have contributed to the description of their cell types based on a flow cytometry
75 approach combined with lectin labelling. While this study provided a basic description
76 of cœlomocyte diversity in *H. scabra*, their functional characterisation requires further
77 investigations.

78 The immune response also involves the expression of a large number of genes coding
79 for different cellular activity regulators and humoral factors. In recent years, RNA-
80 sequencing (RNA-seq) has become a prominent tool for identifying differentially
81 expressed genes (DEGs) following various stresses [10]. In sea cucumbers, and
82 especially in the species *Apostichopus japonicus*, RNA-seq has been notably
83 employed to characterise the immune response of cœlomocytes to different
84 immunological stress including exposure to *Vibrio splendidus*, a common pathogen
85 bacteria of sea cucumbers [11], or lipopolysaccharide (LPS) [12], an endotoxin
86 characteristic of Gram-negative bacteria that is commonly used to generate an immune
87 response [12]. While these few studies all point to great complexity in the immune

response in holothuroids, the number of such transcriptomic studies and the diversity of species investigated remains limited.

The present study aimed to morpho-functionally describe the cœlomocytes of *H. scabra*. Firstly, the different types of cœlomocytes were characterised using scanning electron microscopy (SEM) and transmission electron microscopy (TEM) and a comparison of the cell population was carried out between the HF and the PF. Secondly, the immune response of cœlomocytes was studied 24 hours after an LPS injection by investigating the change in the cœlomocyte population and identifying the immune gene expression using *de novo* RNA-seq, which was then confirmed by cDNA amplification and gel electrophoresis on a selection of six immune genes. Overall, our results provide a general overview of the immune response in *H. scabra*, from the molecular to the cellular level, and will contribute to a better understanding of immune mechanisms in holothuroids.

2. Material and Methods

2.1. Specimen collection and handling

Specimens of *Holothuria scabra* Jaeger, 1833 were collected in the sea pens of the Indian Ocean Trepang (IOT) company (sea cucumber aquaculture) in Belaza (23°29’13.2"S; 43°45’32.4"E) and Andrevo (23°01’15.6"S; 43°31’22.8"E), in Madagascar, in November 2019 and April 2024 (**Fig. 1**). They were harvested by hand and by snorkelling during night time (between 1 and 2 m deep at high tide, seawater temperature = 26.5°C) to induce as little stress as possible. On the boat, they were directly placed in seawater tanks before being brought back to the *Institut Halieutique et des Sciences Marines* (IH.SM) of the Toliara University where they were kept in tanks of 1 µm-filtered seawater (pH = 8.5; salinity = 34 psu; and temperature = 26°C).

All used specimens were initially born within hatcheries of the IOT company, requesting no specific permissions for this study on endangered organisms.

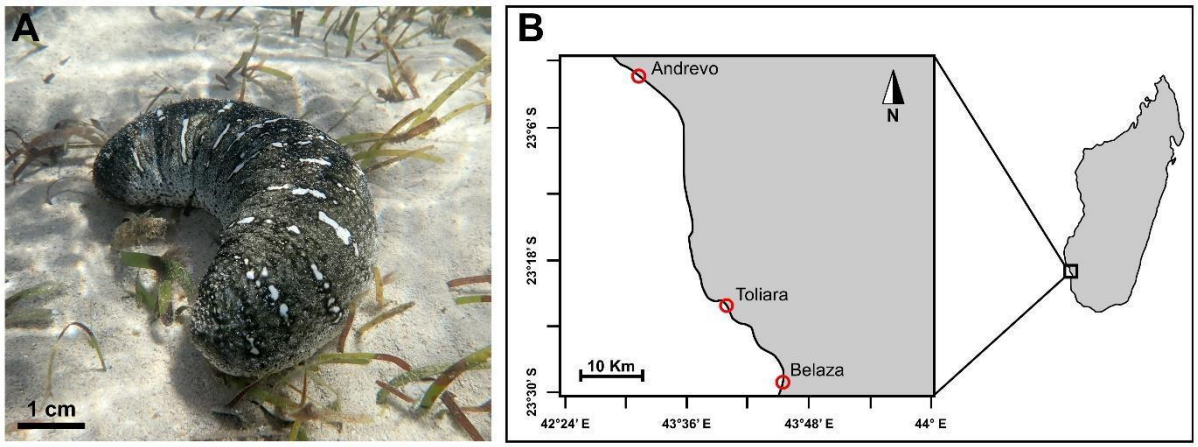

Fig. 1. *Holothuria scabra* in Madagascar. A. Picture of an *in-situ* specimen. B. Map illustrating the different collection sites in the sea pens of the IOT company (Andrevo and Belaza) and the place where specimens were preserved for the study (*Institut Halieutique et des Sciences Marines* in Toliara).

2.2. Cœlomocyte harvesting and processing

Cœlomocytes were harvested from two body fluids: the perivisceral fluid (PF) and hydrovascular fluid (HF). Initially, a longitudinal incision was carried out on the *bivium*, from the posterior to anterior part, to open the perivisceral cavity and collect the PF. Then, the Polian vesicle was isolated and poured to harvest the HF. Depending on the following process, cœlomocytes were either directly observed under a microscope or mixed with an equivalent volume of artificial cœlomic fluid (aCF) (25 mM dithiothreitol; 10 mM $CaCl_2$; 50 mM MCl_2; 14 mM KCl; 398 mM NaCl; 1.7 mM $NaHCO_3$ and 25 mM Na_2SO_4; pH = 7.4) as per Smith et al. [13].

2.3. Cœlomocyte morphotype description

2.3.1. Light microscopy and morphotype abundance estimation

To establish the concentration and proportion of each cell type in a normal homeostasis state, the HF and PF of 9 individuals from two different aquaculture sites were collected (4 from Andrevo and 5 from Belaza; **Fig. 1B**). Then, 10 µL of each body fluid was

loaded on a Neubauer hemacytometer and the 16 subdivisions of the slide, corresponding to a total volume of 0.1 mm^3, were photographed under a microscope (CX41, Olympus). Cœlomocyte morphotypes were identified based on previous cœlomocyte descriptions in other sea cucumber species [4,8] and were counted manually using the ImageJ software (V1.40g). Cell concentrations were converted in million cells per ml and the results were formulated as mean ± standard deviation (SD). Proportions were calculated as the number of cells of the morphotype considered out of the total number of coelomocytes (all morphotypes together) and converted into percentages. To reveal any relation in the concentration and proportion of cœlomocytes between the two body fluids of the different individuals, a statistical analysis was performed on Prism software (V5.03): firstly, a paired statistical test was carried out to reveal potential differences (Wilcoxon matched pair signed rank test; $\alpha = 5\%$); secondly, a correlation test was achieved to reveal a potential correlation between the two fluids (Pearson correlation; $\alpha = 5\%$). Furthermore, a statistical test was performed to highlight potential site-specific differences in coelomocyte proportions and concentrations (between Andrevo: n = 4 and Belaza: n = 5; Mann Whitney test; $\alpha = 5\%$).

2.3.2. Scanning Electron Microscopy (SEM)

The PF and the HF were immediately mixed with the aCF solution and centrifuged at 500 x g at room temperature for 5 minutes. Pellets were then suspended in 1 ml of a culture medium (500 mM NaCl; 5 mM $MgCl_2$; 1 mM EGTA and 20 mM of HEPES; pH = 7.2) as per Smith et al. [13], and 150 µl were deposited on pre-cut histological slides of 25 mm^2. The slides were incubated in a humid chamber for 30 minutes, following the same protocol [13], so that cœlomocytes could adhere to the slides. After that, cœlomocytes were fixed successively in a prefix solution (0.001% glutaraldehyde in

159 the culture medium; pH = 7.2) for 5 minutes and in a fixative solution for 1 hour (3%
160 glutaraldehyde, 0.1 M sodium cacodylate and 1.5% NaCl; pH = 7.4). Once fixed, slides
161 were rinsed in five successive baths of phosphate-buffered saline (PBS; 137 mM NaCl;
162 2.7 mM KCl; 10 mM Na_2HPO_4; 1.76 mM KH_2PO_4; pH = 7.4) and distilled water. Then,
163 cœlomocytes were dehydrated through a series of seven successive ethanol baths
164 with increasing concentrations (3 baths at 70% for 30 minutes, 1 night for 30 minutes;
165 2 baths at 90% for 30 minutes and 1 bath at 100% for 1 hour) and chemically dried in
166 six successive baths of hexamethyldisilazane (HMDS) of increasing concentration in
167 ethanol (1 bath at 33%; 1 bath at 50%; 1 bath at 66% and 3 baths at 100%), the last
168 bath being let evaporated overnight under a fume hood. Once dried, slides were coated
169 with mixture of gold and palladium (40% and 60%, respectively; JFC-1100E metalliser,
170 Jeol) and observed and photographed with a scanning electron microscope (JSM-
171 7200F, Jeol).

172 2.3.3. Transmission Electron Microscopy (TEM)

173 PF and HF were immediately mixed to an equal volume of the aCF solution and
174 centrifuged at 900 x g at room temperature for 2 minutes. The pellets were suspended
175 in the same cold fixative solution as for the SEM (see 2.3.2.) and stored at 4°C. After
176 three rinsing of 10 minutes with a cacodylate buffer (*i.e.* successive centrifugations and
177 pellet suspensions; 0.1 M sodium cacodylate and 1.5% NaCl; pH = 7.4), the pellets
178 were post-fixed in 1% osmium tetroxide in the same cacodylate buffer. Pellets were
179 once again rinsed three times for 10 minutes in the cacodylate buffer before a
180 dehydration step with 7 successive ethanol baths of increasing concentration (1 bath
181 at 25% for 10 minutes; 1 bath at 50% for 10 minutes; 1 bath at 70% for 20 minutes; 2
182 baths at 90% for 15 minutes; 2 baths at 100% for 30 minutes). Samples were then
183 embedded in Spurr resin. Finally, ultrathin sections (90 nm thick) were cut using an

ultramicrotome (Leica UCT) equipped with a diamond knife, collected on copper grids, and contrasted with uranyl acetate for 45 minutes and lead citrate for 4 minutes and 30 seconds, successively. Samples were observed and photographed with a transmission electron microscope (LEO 906E, Zeiss).

2.4. Immune response

2.4.1. Variation in cœlomocyte morphotype concentration

To identify modifications in cœlomocyte populations after the injection of lipopolysaccharides (LPS) three conditions were considered: a LPS injection group (n = 4), inoculated with 100 µL of sterile seawater containing 5 mg/ml of LPS from *Escherichia coli* O111:B4 (L2630; Sigma-Aldrich); a control injection group (n = 4), inoculated with 100 µL of sterile seawater and a no injection group (n = 4), receiving no injection. The injections were carried out using a 1 ml syringe and a 23 g needle in the right anterior part. Specimens used for this experimentation were all collected at the same location in Andrevo and were kept 24 hours in a tank before the experimentation. PF and HF were collected 24 hours after the injections to quantify the cœlomocytes on a hemacytometer and the concentration of each cell type was calculated as explained above (see 2.3.1). Finally, a two-by-two statistical test was performed in Prism software (V5.03) to reveal potential significant differences between the three different conditions (Mann Whitney test; $\alpha = 5\%$).

2.4.2. Transcriptomic analysis of the immune response to LPS

2.4.2.1. Immunostimulation and cœlomocyte processing

Transcriptomic analysis was carried out on cœlomocytes from PF and two conditions were compared for the final purpose of identifying the immune differentially expressed genes (IDEGs): a LPS injection group as test condition (n = 3) and a control injection group as a control condition (n = 3). All specimens came from the same sea pen in

209 Andrevo and were kept 24 hours in a tank before the experimentation. Coelomocytes
210 from the PF have been shown to have a wide range of immune gene expression
211 [11,12,14], and PF is easier to collect in larger volumes compared to PF. Hence, the
212 transcriptomic analysis was focused on the PF. Injections were carried out in the same
213 way as for the study of variation in cœlomocyte populations (see section 2.4.1.), 24
214 hours before collecting the PF. Once isolated, the PF was directly mixed with the same
215 volume of the aCF to avoid the clotting of cœlomocytes and the mixture was
216 centrifuged at 500 x g for 5 minutes at room temperature. Pelleted cells were then
217 suspended in RNAlater® (R0901; Sigma-Aldrich) and stored at 4°C until their transfer
218 to the Belgian laboratory (University of Mons). There, the tubes were centrifuged again
219 at 500 x g at 4°C for 5 minutes to remove the RNAlater® and the pellets were stored
220 at -80°C until RNA extraction.

221 *2.4.2.2. RNA extraction, cDNA library preparation and sequencing*

222 RNA extractions were performed using the RNeasy Mini kit (Qiagen) following the
223 manufacturer's instructions. The concentration and purity of the extracted RNA were
224 determined using a microspectrophotometer (Denovix DS11) and the RNA integrity
225 value (RIN) was assessed using the Agilent 2100 Bioanalyzer (Agilent RNA 6000 Nano
226 kit). The preparation of cDNA libraries and the sequencing were performed by the
227 Beijing Genomics Institute (BGI, Hong Kong). Briefly, cDNA libraries were built as
228 follows: mRNAs were isolated from total RNA using the oligo(dT) method; purified
229 mRNAs were fragmented, and reverse transcribed into the first strand of cDNA, before
230 the synthesis of the second strand of cDNA; double-stranded cDNA fragments were
231 end-repaired, 3'-adenylated and connected with Illumina adapters; cDNA fragments of
232 appropriate size were selected and enriched by PCR. After validation using the Agilent

2100 Bioanalyzer, the library was sequenced using the Illumina HiSeq™ 2000 sequencer and the resulting raw reads were retrieved in FASTQ format.

2.4.2.3. Raw data filtering and De novo *assembly*

Before the assembly, raw reads were filtered to remove adapter-polluted reads, reads containing more than 5% of unknown bases and low-quality reads (*i.e.* reads comprising more than 20% of bases with a quality value of less than 10). The transcriptome was assembled *de novo* using the Trinity software (V2.0.6). The resulting transcripts were then clustered using Tgicl software (V2.0.6) to eliminate redundancy and obtain the final sequences called unigenes. The unigenes can either form clusters comprising several unigenes with more than 70% overlapping or singletons (*i.e.* single unigenes). As the sequence length is a criterion of the assembly quality, the size distribution of unigenes was represented.

2.4.2.4. Transcriptome completeness and functional annotation

To assess the completeness, BUSCO statistic was assessed for each individual transcriptome and the merged results using the tool BUSCO in the Galaxy server (https://usegalaxy.eu; V5.4.6). The BUSCO metrics attempt to provide a quantitative assessment of the completeness of genomics data by classifying orthologs into the four following categories: complete and single-copy, complete and duplicated, fragmented, or missing BUSCOs [15].

To have a first indication of the unigene function, the sequence of each unigene was aligned against several protein databases including NCBI NT (http://www.ncbi.nlm.nih.gov.), NCBI NR (http://www.ncbi.nlm.nih.gov.), GO – Gene Ontology (http://www.geneontology.org), KOG – EuKaryotic Orthologous Groups (http://.ncbi.nih.gov/pub/COG/KOG), KEGG – Kyoto Encyclopedia of Genes and

Genomes (http://www.genome.jp/kegg), SwissProt (http://www.ebi.ac.uk/pub/databases/swissprot) and InterPro (http://www.ebi.ac.uk/interpro) using BLAST (V2.2.23), Diamond (V0.8.31), Blast2GO (V2.5.0) and InterProScan5 (V5.11-51.0). The annotation of unigenes provides an e-value that quantifies the degree of annotation reliability: only annotations with an e-value < 10^{-5} were considered. Overall, the NR annotation was preferred, except for some unigenes for which the SwissProt annotation resulted in a gene having a specific function in immunity that was not revealed by NR annotation (see section 2.4.2.7). Moreover, the distribution of species among the Nr annotations was assessed to highlight similarities with existing genomic data.

2.4.2.5. Gene expression level and identification of the differentially expressed genes

The expression level of each unigene was calculated following the “Fragments per kilobase of transcripts, per million mapped reads” – FPKM method. FPKM is an informative expression value that integrates the influence of the sequence length as well as the sequencing level but does not directly inform about differential expression. The differentially expressed genes (DEGs) were identified using the DESeq2 package. The result consists of a fold change value which corresponds, for a given unigene, to the ratio of the mean expression level between the test and the control conditions. The fold change values (FC) were formulated as $\log_2$ for easier readability. In addition to the FC, DESeq2 performed a Wald statistical test to check the significance of the differential expression. The generated p-value is adjusted following the Benjamini–Hochberg procedure and called the False Discovery Rate (FDR). Only the unigenes having a $|\log_2(\text{FC}) \text{ value}| \geq 1$ and an FDR ≤ 5% were considered as significantly differentially expressed.

To represent the differential expression between the two conditions, the DEG FPKM values were loaded in MetaboAnalyst (V5.0). After a $\log_{10}$ transformation and autoscaling (mean-centred and divided by the SD of each DEG), a heatmap of DEGs as well as a correlation matrix of individuals was constructed to represent the differential expression and the individual heterogeneity, respectively.

2.4.2.6. Functional classification and enrichment analysis of GO terms and KEGG pathways

The GO and KEGG databases are useful bioinformatic resources which provide a standardised classification of genes and proteins according to their ontology or biological pathways, respectively. These databases were used to provide a general functional description of the DEGs via enrichment analyses. Furthermore, KEGG pathway enrichment was used to identify the ten most enriched pathways, all categories included, as well as the ten most enriched pathways among the KEGG organismal system “immune system”.

2.4.2.7. Identification of immune DEGs

The immune DEGs (IDEGs) were identified based on their functional annotations. Primarily, the KEGG pathway enrichment was used to provide the list of DEGs that correspond to "immune systems" among the different organismal system pathways. Secondly, a "keyword search" was performed among the DEG annotation list to find genes of interest that were selected from different immune gene atlas in echinoderms [4,16,17]. The results of these two searches were combined and only the most relevant genes to the literature are presented in the results (see 3.2.2.5). This list was represented as a heatmap: the gene expression was transformed as in 2.4.2.5. and these values were extracted to build the final figure in Excel. IDEGs were classified

according to their presumed function to facilitate the readability and therefore, no clustering was performed on this heatmap.

2.4.2.8. Validation of the differential expression by cDNA amplification and gel electrophoresis

To appreciate the reliability of the differential expression analysis performed using RNA-seq, a second independent experimentation was carried out following the same experimental design: 5 individuals injected with LPS and 5 individuals injected with sterile seawater. After the perivisceral coelomocyte collections and RNA extractions, cDNAs were obtained for all samples using the qScript cDNA supermix kit (Quantabio). All cDNAs were quantified using a microspectrophotometer (Denovix DS11). PCR amplification was subsequently carried out using the Red'y' Star PCR Mix (Eurogentec) on a selection of immune genes. Custom primers were designed using the Primer3 webtool (V. 4.1.0) and purchased using the commercial services of Sigma-Aldrich. cDNA amplicons were loaded on a 1.2% agarose TBE gel electrophoresis for migration and were then immersed in 0.03% of gel red TBE during 45 minutes. Gels were then photographed under UV light, and the band intensity of each sample was quantified using tool “Gel” in the software ImageJ (V. 1.54f) to calculate a fold change value between the two conditions. To do this, six immune genes were selected as well as one control gene (**Table 1**), namely the 16S RNA gene as per [18], to ensure a similar level of expression between the different samples, enabling their comparison. The degree of correspondence between the two techniques was finally determined using linear regression in Prism (V5.03) (coefficient of determination and F-test; $\alpha = 5\%$).

Table 1. Primers designed for transcriptome validation by cDNA amplification and gel electrophoresis.

Gene_ID	Annotation	Forward primer	Reverse Primer
CL2676.Contig3	Interleukin 17-like	GGTAATTCACTGGGCAGGCT	ATGGACTTGCACGGAGAAGG
CL6562.Contig1	ADAMTS	TTGTCGAAGGTGTGATGGGG	TCTCCGGCATTACATCGTCG
Unigene16245	Laccase-type phenoloxidase	CGCTTTCCTCGCTCTACAGT	AGGAGCAGACCAGGCATCTA
Unigene9113	NLRP10	CCTGTTTTGCCACGAACCTG	CCCGTGGTGATAAAGGAGGG
CL11782.Contig7	NLRP10	TGCGCTTTCTTGCTCCTACA	GGCCTTTCTTCCTCCACACA
CL10116.Contig2	Coagulation factor VII	ACAGACCCCAGCATTGACAG	GGCAGTGTCTCCTCCTTCAC
Control gene	16S RNA	(16S Ar) CGCCTGTTTATCAAAAACAT	(16S Br) CTCCGGTTTGAACTCAGATC

3. Results and Discussion

3.1. Cœlomocyte diversity

3.1.1. Morphological description of cœlomocyte types

Ten coelomocyte morphotypes were identified based on their morphological characteristics, comprising five main types distinguishable by light microscopy and five subtypes characterized by their ultrastructural features. The five main morphotypes include phagocytes, small round cells (SMCs), spherulocytes, fusiform cells, and crystal cells.

Phagocytes were recognised by their numerous pseudopodia and their strong adhesion to the slide (**Fig. 2A**). They were the largest cœlomocyte type with a diameter measuring between 15 and 40 µm when considering pseudopodia, for a cell body ranging from 4 to 10 µm (*i.e.* without pseudopodia). Phagocytes are traditionally classified into two subtypes based on the shape of their pseudopods: filopodial phagocytes bearing long and thin pseudopods called filipodia and petaloid phagocytes bearing veil-like pseudopods called lamellipodia [19]. Although the two subtypes were observed (**Fig. 2B** and **2C**, respectively), most phagocytes appeared to be an intermediate between the two subtypes (*i.e.* they possessed both lamellipodia and filopodia; **Fig. 2A**), and this is why no distinction has been made in the cell count. This

observation supports the hypothesis that these two types are two different stages capable of transforming from one to the other, rather than distinct functional cell types. Concerning their ultrastructure, only filopodial phagocytes were recognisable based on their filopodia; they showed a large heterochromatic nucleus with peripheral mitochondria and several lysosomes (**Fig. 3A**).

The small round cells (SRCs) measured between 4 and 6 µm (**Fig. 2D**), and their ultrastructure consisted of a large nucleus occupying most of the cellular volume with a dense cytosol containing many mitochondria (**Fig. 3B**). The same cell type was observed in other species of holothuroids and referred to as either progenitor cells [6] or lymphoid cells [20]. The name “progenitor cells” was given because their undifferentiated appearance suggests they could be stem cells, giving rise to the other types of cœlomocytes, while the name “lymphoid cells” was attributed according to a resemblance to vertebrate lymphocytes. However, to date, the functions associated with these cells remain to be demonstrated, and this is why we have preferred a non-speculative name based only on their morphology.

Spherulocytes were identified through their numerous secretory granules (**Fig. 2E**). Their diameter was highly variable, ranging from 5 to 20 µm. Based on their ultrastructure, we were able to distinguish four subtypes: type I spherulocytes were the smallest in diameter (5 - 9 µm) and showed homogeneous, electron-dense secretory granules measuring between 0.5 and 1 µm (**Fig. 3C**); type II spherulocytes were the largest (11 - 20 µm) and also had the biggest secretory granules (3 - 4.5 µm), showing an electron-dense inner part and a loose outer part (**Fig. 3D**); type III spherulocytes had an intermediate diameter (9 - 10 µm) and their secretory granules, measuring between 1.2 and 1.5 µm, were filled of a electron-translucent fibrous material (**Fig. 3E**); type IV spherulocytes were between 10 and 14 µm in diameter and had the highest

number of granules (> 80) but also the smallest (0.3 - 1 µm) (**Fig. 3F**), which were electron dense. The nuclei were similar between the four sub-types; they were irregularly shaped and measured between 1 and 4 µm. In terms of proportion, the two first types were predominant while the two last were less represented on the thin sections. The first three cell types seem to correspond to those observed in TEM in *Holothuria poli*, *A. japonicus* and *C. japonica* with a few size differences [6,21]. Furthermore, Queiroz et al. [22] recently showed that it was possible to distinguish different types of spherulocytes *sensu lato* according to the diameter of their cytoplasm and their secretory granules in three species of the genus *Holothuria*. According to their classification, type II spherulocytes would correspond to morula cells; type III spherulocytes to acidophilic cells and type IV spherulocytes to spherulocytes *sensu stricto*, but no cell type seems to correspond to type I spherocytes. Several studies suggest that the different subtypes of spherulocytes are rather different stages of maturation than true functional cell types [6,21]. For example, Eliseikina and Magarlamov [6] also described "young morula cells" which are relatively small spherulocytes containing many granules. This type of spherocyte is thought to be the primitive stage and is more likely to correspond to type I or type IV spherulocytes based on their size, appearance, and number of secretory granules. Therefore, this continuum in maturation stages could explain the absence of certain subtypes across the different studies, which could vary according to the homeostasis status of the individuals, or the techniques employed to distinguish the different subtypes.

Fusiform cells were identified by their characteristics two opposite pseudopodia (**Fig. 2F**). In some of them, it was possible to distinguish a transition zone between cytoplasmic projections of the cellular body and the pseudopodia, which was marked by a slight swelling (**Fig. 2F**). In terms of size, their cellular body measured between 3

and 5 µm whereas their total length could exceed 30 µm considering their pseudopodia.

Crystal cells were recognised based on their prismatic shape formed by their crystalline inclusion. Indeed, these crystalline inclusions can take different shapes, thus varying the shape of the cell itself; here, some were more rectangular while others were more extended as in **Fig. 2G**. Their size generally varied from 7 to 14 µm but the most elongated ones could reach 25 µm in length.

These two last cell types could not be observed in TEM, probably because of the difficulty of finding poorly represented cell types in TEM preparations. In SEM, however, the fusiform cells were easily identifiable while the crystal cells were rarely observed. We identified the one in **Fig. 2G** according to its close resemblance in both size and morphology to the crystal cells observed under light microscopy. However, whether it is a crystal cell remains speculative and therefore we preferred to report this cell as a “presumed crystal cell”.

In addition to cœlomocytes recognisable under light microscopy, a cell type was only observed in the TEM preparations and was identified based on its particular ultrastructure; it showed a high number of small vacuoles measuring between 0.2 and 1 µm in diameter, some of which contained residual bodies (**Fig. 3G** and **3H**). These characteristics of vacuolated cells were previously described in the species *A. japonicus* and *Cucumaria japonica* [6]. In these species, vacuolated cells were reported to achieve amoeboid movement and to increase in concentration when foreign particles are injected into the body wall (unpublished data from [6]). Based on their morphology, it was suggested that they could participate in the storage and regulation of calcium ions [6]. Although we do not exclude this hypothesis, the

presence of residual bodies inside some vacuoles, which is reminiscent of phagosome-like structures, plus the fact that their abundance seems to correlate with physiological stress, rather suggest that they would be dehiscent phagocytes that have already phagocytosed foreign bodies. Furthermore, this is consistent with the fact that individuals dedicated to the cœlomocyte morphological description in this study came directly from the natural environment and could be exposed to numerous stressors just before the experiment.

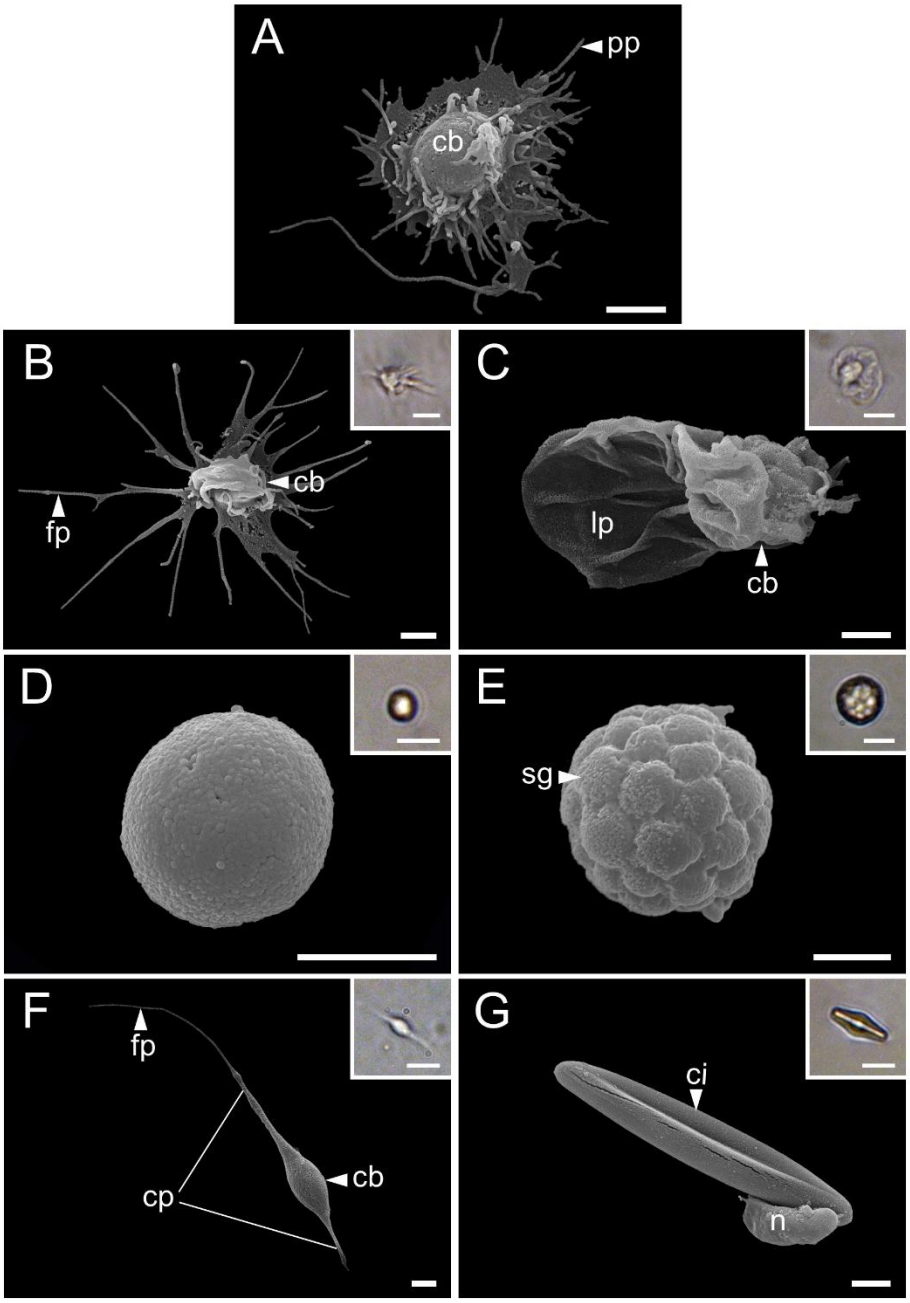

431

432 **Fig. 2.** Cœlomocyte morphotypes in the body fluids of *Holothuria scabra* (light and
433 scanning electron microscopy views). A. Intermediate phagocyte. B. Filiform
434 phagocyte. C. Petaloid phagocyte. D. Small round cell (SRC). E. Spherulocyte. F.
435 Fusiform cell. G. Presumed crystal cell. Legend: cb – cellular body; cp – cytoplasmic
436 projection; ci – crystalline inclusion; fp – filopodia; lp – lamellipodia; pp – pseudopod;
437 n – nucleus; sg – secretion granule. The scale bars represent 2 µm in large images
438 (SEM) and 10 µm in small images (light microscopy).

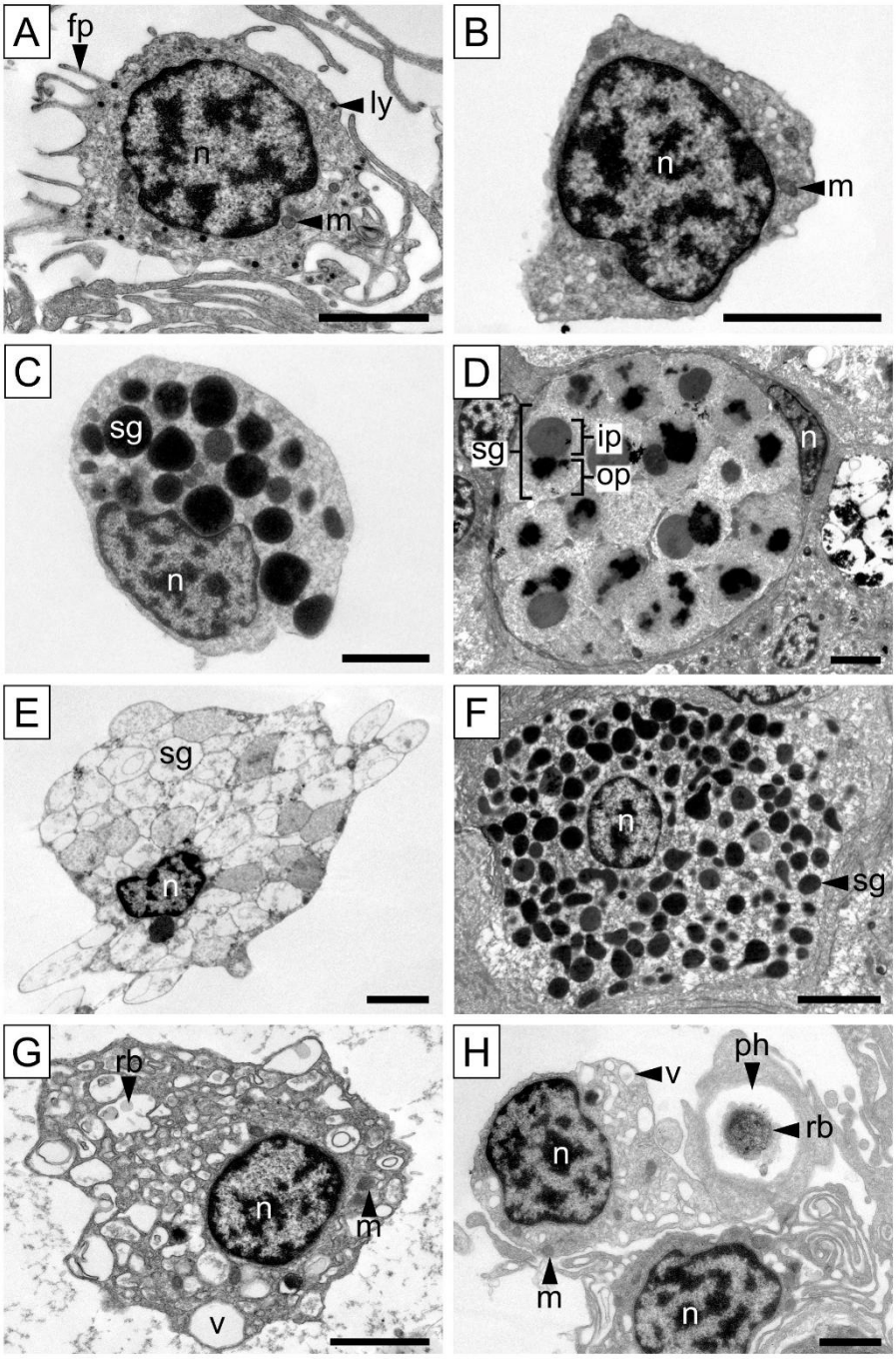

439

440 **Fig. 3.** Ultrastructure of cœlomocyte morphotypes in *Holothuria Scabra* by
441 transmission electron microscopy. A. Filiform phagocyte. B. Small round cell (SRC). C.
442 Type I spherulocyte. D. Type II spherulocyte. E. Type III spherulocyte. F. Type IV
443 spherulocyte. G. Vacuolated cell. H. Vacuolated cell (up-right) and filiform phagocyte
444 (down-left) with a phagosome-like structure containing a residual body. Legend: fp –
445 filipodia. ip – inner part of the granule; ly – lysosome; m – mitochondria; n – nucleus;
446 op – outer part of the granule; ph – phagosome-like structure; pp – pseudopod; rb –
447 residual body; sg – secretory granule; v – vacuole. The scale bars represent 2 µm.

448 3.1.2. Cœlomocyte concentration and proportion in the body fluids of *H. scabra*

449 The total cœlomocyte concentration was 3.5 ± 1.8 10^6 cells ml^{-1} in the HF and 1.7 ±

450 1.2 10^6 ml^{-1} in the PF of *H. scabra* (n = 9). **Table 2** summarises the concentration and

451 proportion values for each of the 5 cell types that were identified under light microscopy

452 in the HF and PF. In both fluids, phagocytes were the dominant type with a proportion

453 of 71.5 ± 17.5% and 60.8 ± 24.6%, respectively. These numbers are consistent with

454 the previous report of Prompoon et al. [9] who reported a proportion of 60.2% in the

455 PF of *H. scabra* and also corresponds to the proportion reported in other holothuroid

456 species [5,21,22]. The second most abundant cell type varies across holothuroid

457 species: for example, it is spherulocytes in *H. poli* while it is progenitor cells (here

458 referred to as small round cells (SRCs), see 3.1.1) in the species *Holothuria grisea*

459 ([21] and [22], respectively). In *H. scabra*, we found that SRCs were more abundant

460 than spherulocytes, with a proportion of about 25% in both fluids. Again, this proportion

461 reflects the previous study of cœlomocytes in *H. scabra* that reported a proportion of

462 25.2% in the PF [9]. Spherulocytes accounted for only 3.4 ± 2.3% and 7.0 ± 8.5% in

463 HF and PF, respectively. These proportions are weaker compared to other species of

464 the genus *Holothuria* [21,22], and it is also lower than the 12.8% previously reported

465 in the PF of *H. scabra* [9]. The last two cell types, fusiform cells, and crystal cells were

466 observed in both fluids but not necessarily in all individuals; out of the nine investigated

467 individuals, fusiform cells were observed in the HF of seven individuals (77%) and the

468 PF of four individuals (44%) whereas crystal cells were observed in the HF of three

469 individuals (33%) and the PF of all individuals. The fact that we did not observe them

470 in all individuals does not necessarily mean that they were not always present in the

471 body fluids since both cell types were reported at low concentrations [8,22]. Their

472 absence in some individuals was also reported in other species [19], and it was even

suggested that fusiform cells are restricted to the PF in the species *Cucumaria frondosa* [5]. These two cell types were not reported by Prompoon et al. [9] which could be attributed to the lectin-based flow cytometry approach they employed, making it challenging to identify less abundant cell types accurately. A last cell type could be observed in the body fluids of three individuals (30%) it was a flagellated cell type that would be traditionally attributed to vibratile cells (*e.g.* [4,19]). However, Caulier et al. (2024) [23] have recently shown that this cell type corresponds to contaminating spermatozoa in holothuroids, which are difficult to avoid when collecting body fluids in males and this is why we did not include this non-immune cell type in our study.

Table 2. Concentration and proportion of each cœlomocyte type in the hydrovascular fluid (HF) and perivisceral fluid (PF) of *Holothuria scabra*. Results are formulated as mean ± SD (minimum value – maximum value) (n = 9). The p-values show significant differences between the two body fluids (Wilcoxon paired signed rank test; p-values ≤ 5% are in bold; W is the sum of signed ranks).

	Concentration (cells ml^{-1})			**Proportion (%)**		
Cell types	HF	PF	p-value (W)	HF	PF	p-value (W)
Phagocytes	2.54 ± 1.62 (0.42 – 5.85) × 10^6	9.22 ± 4.47 (4.4 – 14.5) × 10^5	**2.7×10^{-2} (37)**	71.5 ± 17.5 (41.4 – 93.8)	60.8 ± 24.6 (25.1 – 82.2)	0.2 (23)
Small round cells (SRCs)	8.2 ± 9.61 (1.40 – 30.5) × 10^5	6.52 ± 10.11 (0.3 – 32.3) × 10^5	0.26 (17)	23 ± 18.7 (4.1 – 56.6)	28.4 ± 23.4 (4.6 - 68)	0.73 (-7)
Spherulocytes	1.01 ± 0.87 (0.3 – 3.2) ×10^5	1.09 ± 1.52 (0.1 – 5) × 10^5	0.2 (16)	3.4 ± 2.3 (1.1 – 7.3)	7.0 ± 8.5 (0.6 – 28.6)	0.64 (8)
Fusiform cells	4.44 ± 4.27 (0 – 11.1) ×10^4	2 ± 3.42 (0 – 10) × 10^4	0.86 (4)	1.6 ± 1.8 (0 – 5.3)	1.4 ± 2.5 (0 – 5.7)	0.19 (-23)
Crystal cells	4.44 ± 7.26 (0 – 20) × 10^3	4.7 ± 3 (1 – 8) × 10^4	**1.33×10^{-2} (-36)**	0.4 ± 1 (0 – 3.1)	2.8 ± 1.4 (1.1 – 4.9)	**1.76** ×F **10^{-2} (-41)**
Total	3.51 ± 1.81 (0.64 – 6.24) × 10^6	1.75 ± 1.21 (0.65 – 4.75) × 10^6	$7.42\ 10^{-2}$ (31)	100	100	100

3.1.3. Relation between the cœlomocytes of the HF and the PF

Surprisingly, only a few studies have examined cœlomocytes from the HF (*e.g.* [5,23]), and even fewer have compared cœlomocyte abundance and diversity between the two

491 body fluids (*e.g.* [20]). Here, we compared the concentration and proportion between
492 these two fluids and tried to correlate these values to see if there is any influence of
493 individuality on these metrics. Overall, the statistical test reveals no significant
494 difference in the concentration and proportion between the HF and the PF, except for
495 phagocytes in concentration and crystal cells both in concentration and proportion
496 (**Table 2**). The fact that phagocytes differ significantly in concentration but not in
497 proportion is likely because, as the most represented cell type, they follow the variation
498 in the overall total number of coelomocytes, which is also close to the significance in
499 terms of concentration ($p = 7.42 \times 10^{-2}$; $W = 31$). Regarding crystal cells, their higher
500 concentration and proportion in the PF suggest that this cell type is more restricted to
501 this body fluid.

502 The correlation tests between the two body fluids were weak ($r < 6$) and not significant
503 ($p > 5\%$; see **Table 3**) for most cell types. Most of the concentrations were negatively
504 correlated between the two fluids. These negative correlations could reflect a transfer
505 from one compartment to the other. In contrast to other cell types, SRCs had a positive
506 correlation both in concentration and proportion at $r = 0.41$ and $r = 0.68$, respectively,
507 and a significant correlation only for the proportion ($p = 4 \times 10^{-2}$). These cells were
508 previously described as stem cells [6], and the coelomic epithelium and the Polian
509 vesicle, which respectively enclosed the PF and the HF, were reported to be potential
510 haematopoietic tissues [24]. Therefore, the production of SRCs in the PF and HF would
511 be stimulated by the same physiological pathways and would thus be concomitant,
512 explaining these positive correlations. However, this would not be the case for the
513 differentiated cell types that would rather migrate toward the body area where the
514 infection and/or the injury occur(s).

Table 3. Correlation of the concentration and the proportion for each cœlomocyte type between the hydrovascular fluid and the perivisceral fluid of *Holothuria scabra* (r = Pearson correlation coefficient; r^2 = determination coefficient; p-values show significant correlations; p-values ≤ 5% are in bold).

	Concentration			Proportion		
Cell types	r	r^2	p-value	r	r^2	p-value
Phagocytes	-0.59	0.34	0.097	0.56	0.31	0.12
Small round cells (SRCs)	0.41	0.16	0.28	0.68	0.47	**0.04**
Spherulocytes	-0.23	0.05	0.55	-0.06	0.00	0.87
Fusiform cells	-0.15	0.02	0.693	0.14	0.02	0.73
Crystal cells	-0.50	0.25	0.173	-0.32	0.10	0.40
Total	-0.26	0.07	0.508	1.00	1.00	0.00

Overall, we were not able to reveal any clear relation between the HF and the PF, suggesting that the influence of individuality on cœlomocyte concentration and proportion is weak or at least more complex than expected. This conclusion corroborates the previous study of Li et al. [20] that could find much the same cell types in both fluids but failed to demonstrate a clear relationship in the cell type concentration or proportion between the two fluids.

3.1.4. Influence of the aquaculture sites on coelomocyte concentration and proportion

The comparison between the two aquaculture sites can be viewed in **Supplementary Material 1**. Although differences in the concentration and proportion of cœlomocyte types are evident, particularly the significantly higher concentration of spherulocytes in the PF at the Belaza site ($p = 2 \times 10^{-2}$; $U = 0$), the order of morphotypes by concentration and proportion remains consistent between the two aquaculture sites.

This consistency highlights a typical cœlomocyte profile indicative of normal homeostasis.

3.1.5. Cœlomocyte aggregates

The examination of the body fluids also reveals the presence of numerous cellular aggregates that were mainly composed of phagocytes, spherulocytes and SRCs (**Fig. 4A-D**). These aggregates have been termed “early aggregates” because their size and number seemed to correlate with the time elapsed since body fluid collection. Three types of early aggregates could be distinguished according to their size and appearance, probably corresponding to successive stages of maturation: small aggregates, measuring between 20 and 100 µm, were of limited cell number and were completely colourless (**Fig. 4A**); intermediate aggregates, measuring about 100 µm, had some brownish spots and were denser (**Fig. 4B**); large aggregates, measuring between 100 and 200 µm, were fully pigmented and their high density made it difficult to distinguish cells constituting them (**Fig. 4C**). Aggregation of cœlomocytes is usually observed during the body fluid collection and the use of an anticoagulant solution is often necessary to avoid this phenomenon [13]. This aggregation is attributed to the encapsulation process, *i.e.* an important cellular mechanism that consists of entrapping a foreign body in a cellular aggregate [25]. This mechanism is well described in arthropods and involves a melanisation phenomenon that implicates the deposition of melanin within the aggregate [25]. Thus, the colour change that is observed between the three early aggregate stages could be attributed to this melanisation process.

In addition to the early aggregates, large brown aggregates were observed on the inner wall of the Polian vesicle (**Fig. 4E**). These aggregates were much larger than those found in cell suspension with a diameter ranging from 150 to 1000 µm. They appeared to be mainly composed of small cells similar in size to SRCs, but which are coloured,

559 although a few spherulocytes could be observed in some of them (**Fig. 4F**). In contrast
560 to the early aggregates, these brown aggregates seemed to pre-exist the collection of
561 the body fluids and were only observed in the hydrovascular compartment. Such
562 coloured aggregates have been observed in several species of echinoderms and have
563 historically been referred to as brown bodies. Recently, Jobson et al. [26] showed that
564 the colour of these aggregates varied according to the class of echinoderm considered,
565 thus matching the phylogeny of extant echinoderms. Furthermore, Caulier et al. [5]
566 suggested that these aggregates could change in colour depending on the body
567 compartment in which they were found in the holothuroid species *C. frondosa*, ranging
568 from red in the HF to brown in the PF. . The presence of these cells was recently
569 reported in the HF of several species of the genus *Holothuria*, including *H. scabra* [23].
570 However, in *H. scabra* the colour of the cell was brown rather than red. The reason
571 why we could not detect any of these cells in cell suspension could be that, in the
572 immunoquiescent state, these cells remain marginated, *i.e.* attached to the membrane
573 of the adjacent tissues [5]. Hence, a large proportion of hemocytes could have
574 remained attached to the membrane of the Polian vesicle during the HF collection. It
575 has been suggested that the colour of these cells was due to haemoglobin that may
576 vary in colour under certain conditions such as different oxygen concentrations [5].
577 However, to date, there is no formal evidence that this pigmentation is due to
578 haemoglobin and further analyses are required to identify the molecular nature of this
579 brown colour.

580 Overall, while the early aggregates would correspond to the initial stages of
581 encapsulation due to the fluid collection, brown aggregates would rather correspond to
582 the result of this process, or at least to a deposition of particular cells that pre-exists
583 the body fluid collection.

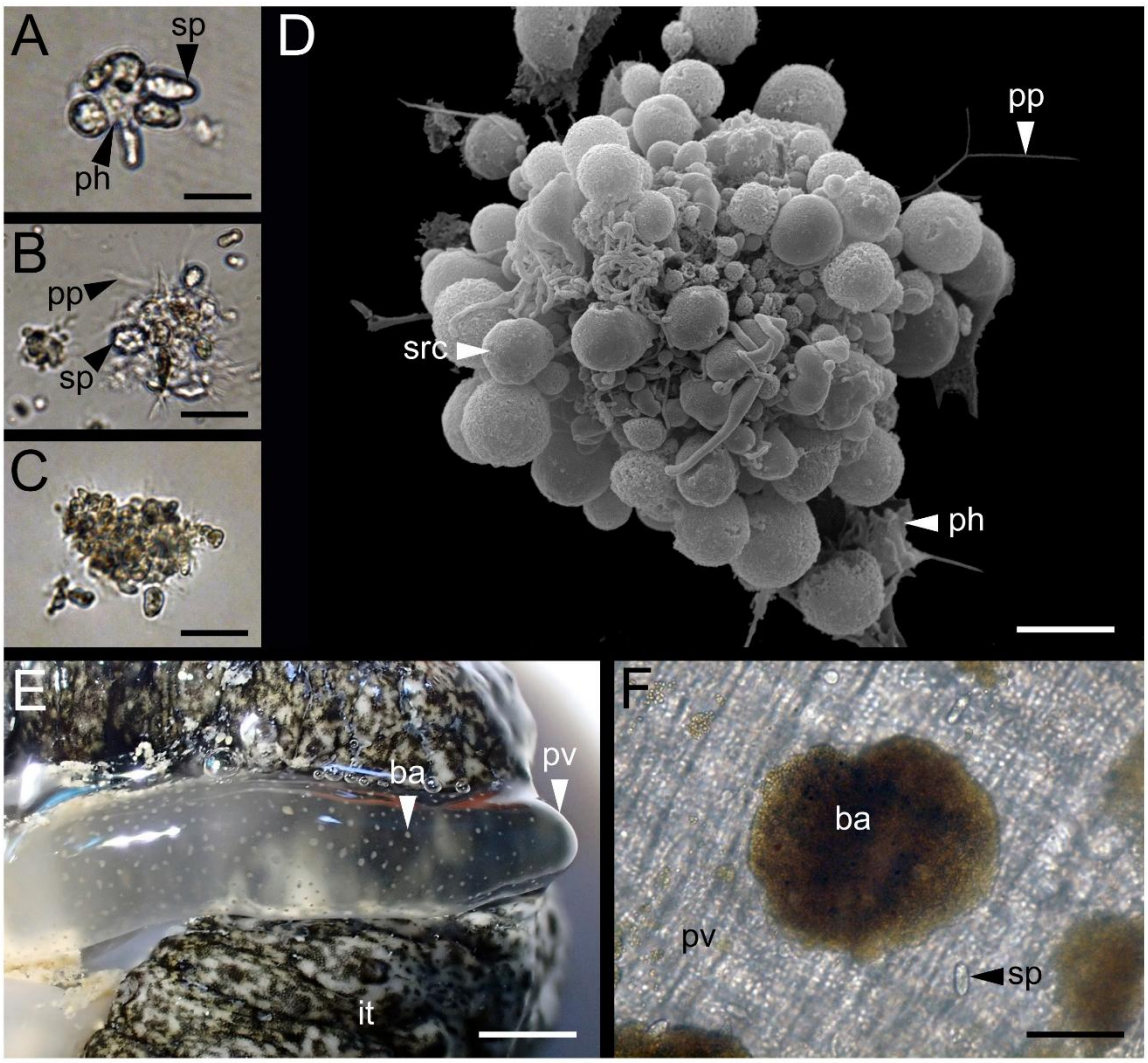

584

585 **Fig. 4.** Cœlomocyte aggregates in *H. scabra*. A. Small uncoloured aggregate. B.
586 Intermediate aggregate harbouring pigmented spots. C. Large aggregate fully
587 pigmented. D. SEM picture of a cœlomocytes aggregate. E. Polian vesicle showing
588 coloured aggregates. F. Optical view of the coloured aggregates on the internal wall of
589 the Polian vesicle. Legend: ba – brown aggregate; it – integument; ph – phagocyte; pp
590 – pseudopod; pv – Polian vesicle; sp – spherulocyte; src – small round cell. The scale
591 bars represent 20 µm in A; 30 µm in B; 40 µm in C; 5 µm in D; 4 mm in E; and 60 µm
592 in F.

593 ### 3.2. Immune response of cœlomocytes

594 #### 3.2.1. Modification in cœlomocyte concentration and proportion

595 The results of the change in coelomocyte concentration between the different
596 conditions do not show a clear change in cell populations. This can be explained by
597 high inter-individual variability, probably encompassing a large part signal from the

598 conditions (**Supplementary Material 1**). This inter-individual variability was particularly
599 noticeable in the group injected with sterile seawater, suggesting a contrasting
600 response to this type of injection between individuals. High variability in injected groups
601 might be partially explained by the fact that, as sea cucumbers are soft-body
602 organisms, it is difficult to ensure the exact location of the injection inside the animals.
603 Thus, although we have tried to inject in the perivisceral cavity, it is possible that
604 different individuals were injected into different compartments, which could have led to
605 these different responses [23]. Despite this, some significant differences were
606 observed between the group without injection and the group with LPS injection,
607 consisting of an increase in SRCs in PF ($p = 2.9 \times 10^{-2}$; $U = 0$) and a decrease in
608 spherulocytes in HF (p = 4 × 10-2; U = 0.5) in the group with LPS injection. However,
609 it is difficult to interpret these results given that the same patterns were not observed
610 in the two fluids. Regarding the proportion of coelomocytes, although variability was
611 still high, especially in seawater-injected individuals, the results were more consistent
612 between the two fluids with a decrease in the proportion of phagocytes concomitant
613 with an increase in the proportion of SRCs (Fig. 5) in the injected conditions (*i.e.* control
614 and LPS injection). SRCs are thought to be progenitor cells that can differentiate into
615 other types of coelomocytes [6]. Their production could therefore be stimulated to
616 compensate for the loss of effective immune cells such as phagocytes. In addition,
617 spherulocytes were significantly less numerous in the HF of the LPS-injected group
618 than in the non-injected group ($p = 2.9 \times 10^{-2}$; $U = 0.5$). Spherulocytes play an important
619 role in the immune response, particularly in the production of various humoral factors,
620 encapsulation and wound healing [4]. Their lower concentration and proportion in the
621 LPS-injected group could be explained by their involvement in the immune response,

622 which could lead to an apoptotic process following degranulation or participation in
623 cellular aggregates.

624 Overall, these results reflect the large inter-individual variability in coelomocyte
625 populations, suggesting complex and rapid regulatory mechanisms in coelomocyte
626 production and activation. They also indicate that coelomocyte counting is not
627 necessarily the best indicator for assessing stress in *H. scabra*, or at least that its use
628 requires many individuals. At the very least, as it has been shown that holothuroids
629 can rapidly modulate their water content in response to environmental stress [28], we
630 recommend using proportion as an indicator, which does not depend directly on the
631 volume of fluid in the organism.

632

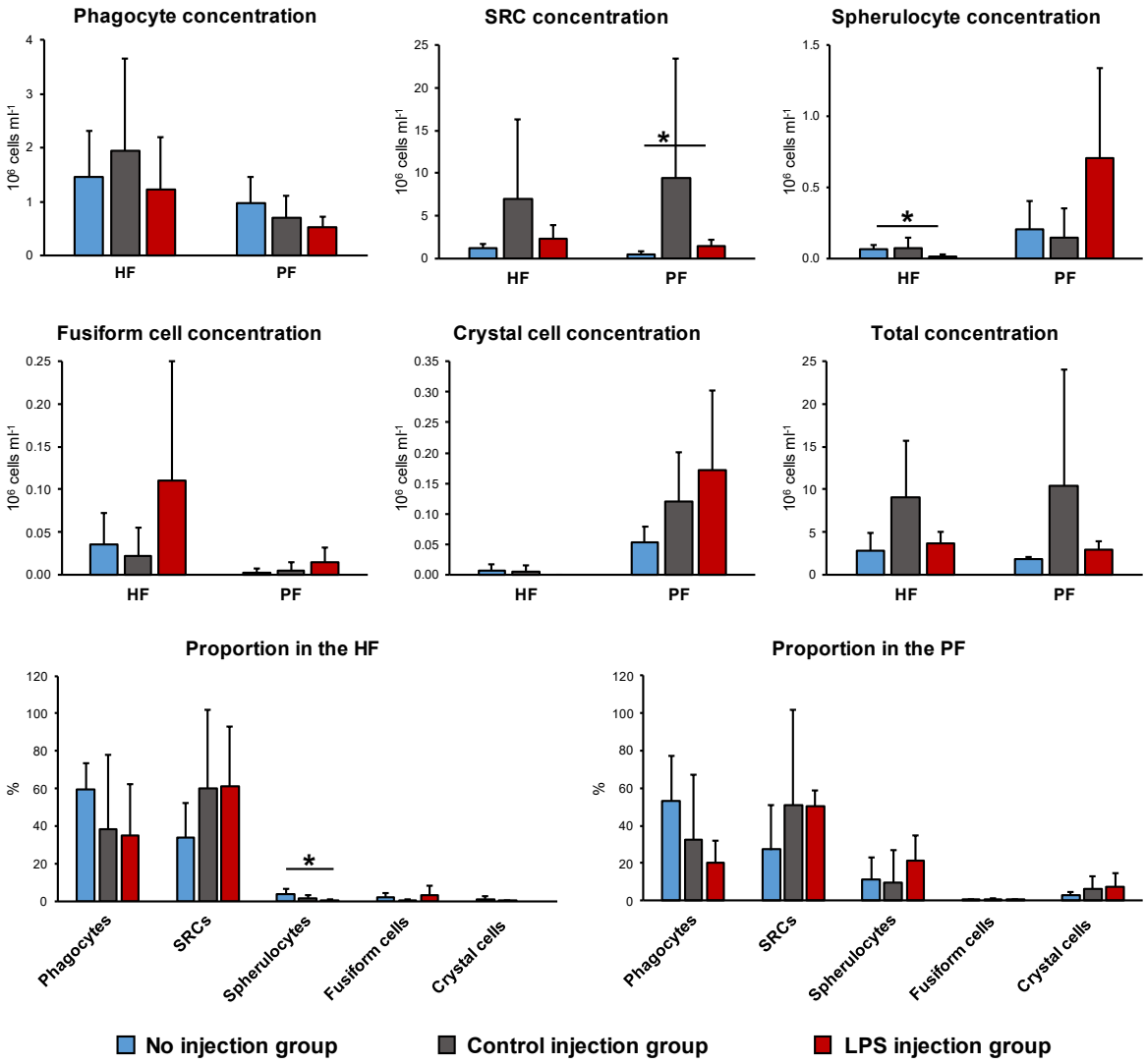

633

634 **Fig. 5.** Cell concentration and proportion fluctuations 24 hours after control and
635 lipopolysaccharide (LPS) injections for each cœlomocyte type in the hydrovascular
636 fluid (HF) and perivisceral fluid (PF). The no injection group received no injection; the
637 control injection group received control injections of sterile seawater; and the LPS
638 injection group received injections of sterile seawater containing lipopolysaccharides
639 (n = 4 in each condition). Results are formulated as mean ± SD and the asterisks (*)
640 represent significative differences (Mann-Whitney test; $p \leq 5\%$)

641

642

3.2.2. Immune gene expression

3.2.2.1. De novo *assembly and quality assessment*

To identify the immune genes in *H. scabra*, the PF cœlomocyte gene expression was compared between LPS injection individuals (test group; n = 3) and control injection individuals (control group; n = 3). The six cDNA libraries sequenced yielded a total of 98.34 Gb of bases with a total of raw reads per sample ranging from 87.47 M to 143.07 M. After filtering and *de novo* assembling all the samples, we obtained a transcriptome of 162,703 unigenes with a total length of 171,636,263 bp, an average length of 1,054 bp, an N50 of 3,241 bp and GC proportion of 38.42%. **Table 4** summarizes the quality metrics of the clean reads and unigenes for each individual transcriptome. The number of unigenes per individual ranged from 85,950 to 101,825 with most of them having a length between 300 and 3000 (**Fig. 6A**).

Table 4. Quality metrics of clean reads and unigenes for each individual replicate; CON – control injection; LPS – LPS injection; R – replicate number.

Replicates	CON-R1	CON-R2	CON-R3	LPS-R1	LPS-R2	LPS-R3
Reads						
Total raw reads (MB)	124.94	142.15	112.66	143.07	107.81	96.19
Total clean reads (MB)	113.14	128.04	102.82	128.15	96.03	87.46
Total clean bases (GB)	16.97	19.21	15.42	19.22	14.4	13.12
Clean reads Q20 (%)	98.3	98.3	98.3	98.3	98.3	98.3
Clean reads ratio (%)	90.6	90.1	91.3	89.6	89.1	90.02
Unigenes						
Total number	90,695	101,825	85,950	90,020	89,967	86,535
Total length (Mbp)	77.36	81.84	60.41	76.39	69.83	72.21
Mean length (bp)	853	803	702	848	776	834
N50 (bp)	1,610	1,473	1,147	1,668	1,505	1,661
GC (%)	38.4	38.5	38.3	38.5	38.5	38.4

3.2.2.2. Completeness evaluation and general functional annotation

BUSCOs were evaluated to assess the completeness of individual transcriptomes and the merged transcriptome (**Fig. 6B**). For the individual transcriptomes, the BUSCO percentage ranged from 54.8% (CON-R3) to 76.9% (LPS-R1) of complete BUSCOs (complete and duplicated single copies); from 13.2% (LPS-R1) to 24.2% (CON-R3) of fragmented BUSCOs; and from 8.3% (CON-R1) to 21.0% (CON-R3) of missing BUSCOs. The percentages for the merged transcriptome were 94.5% complete BUSCOs (59.5% complete single copies and 35.0% copies); 3.2% fragmented BUSCOs; and 2.2% missing BUSCOs. While the individual transcriptomes showed variable degrees of completeness, the merged transcriptome showed a low proportion of fragmented and missing BUSCOs (3.2% and 2.2 %, respectively), indicating an overall good assembly quality, especially considering that coelomocytes are highly specialised cells [15].

To obtain a first functional indication, each unigenes were aligned to seven functional databases: 43,976 unigenes (27.03%) matched significantly to at least one database (E-value < 10^{-5}) and 2,899 (1.78%) to the seven databases. Nr was the database that matched the highest number of unigenes with 36,954 annotated unigenes (22.71% of all unigenes), followed by InterPro (29,966; 18.42%) and KEGG (29,518; 18.14%) databases (**Fig. 6C**). For the NR annotation, the species distribution of unigenes was 36.98% in *Acanthaster planci* (Asteroidea), 25.76% in *Strongylocentrotus purpuratus* (Echinoidea), 4.03% in *Saccoglossus kowalevskii* (Hemichordata), 2.34% in *A. japonicus* (Holothuroidea) and 30.69% for other species (**Fig. 6D**). General functional distribution of KOG, GO and KEGG annotations can be consulted in **Supplementary Material 3**.

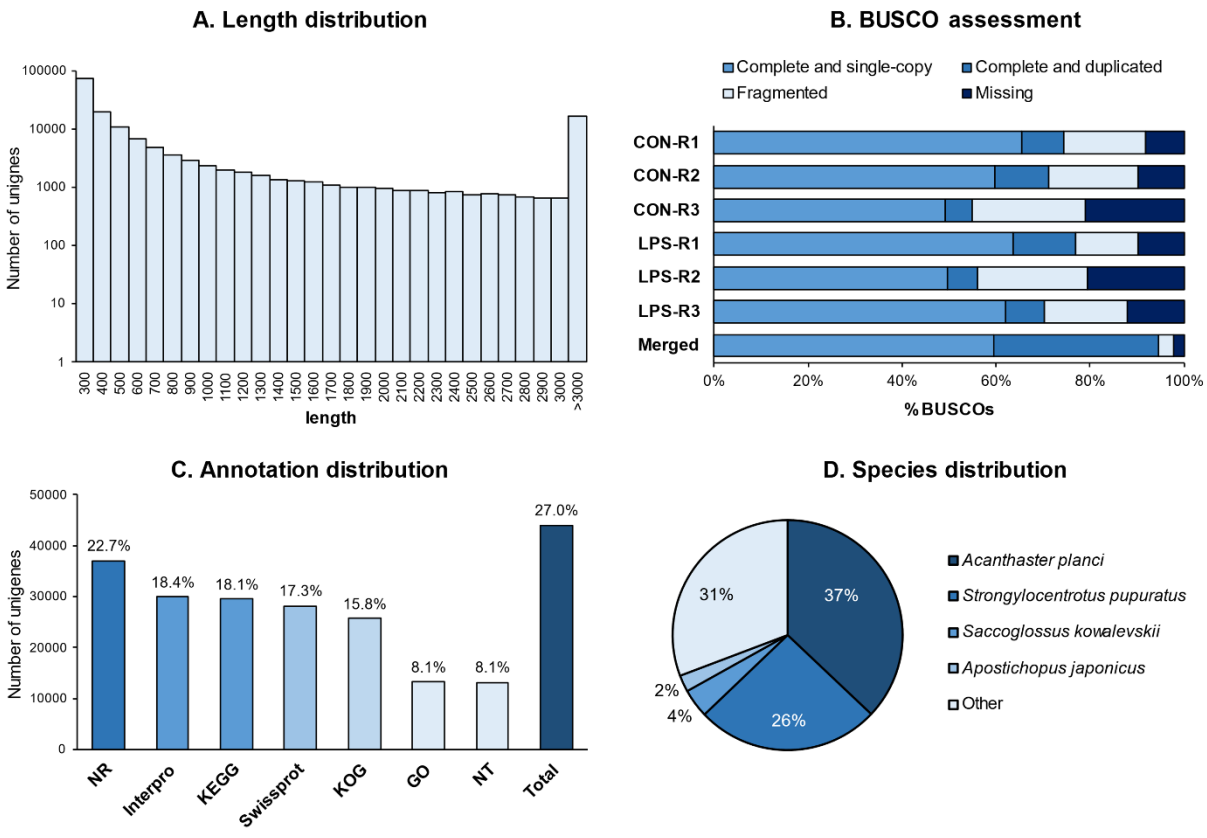

684

685 **Fig. 6.** Quality assessment and functional annotation metrics of the coelomocyte
686 transcriptome of *H.* scabra. A. Length distribution of unigene sequences of the merged
687 transcriptome (in bp; the number of unigenes is embedded in the graph). B. BUCO
688 assessment graph (CON-R – control injection replicates; LPS-R – LPS injection
689 replicates). C. Proportion of annotated unigenes for each functional database (the
690 percentage of annotated unigene is embedded in the graph). D. Species distribution
691 for the Nr annotation with the respective percentage for each species.

692

693 *3.2.2.3. Identification of differentially*

694 *expressed unigenes (DEGs) after the LPS injection*

695 A differential expression analysis was performed to identify the differentially expressed
696 genes (DEGs) between control injection and LPS injection individuals (FDR ≤ 5% and
697 a $|\log_2 \text{fold change}| \geq 1$). In total, 945 DEGs were obtained (0.77% out of all unigenes),
698 including 673 up-regulated unigenes and 272 down-regulated unigenes in the LPS
699 injection individuals (**Fig. 7A**). A clear positive correlation was found between individual
700 replicates from the same condition and a negative or weak correlation between
701 individuals from the two different conditions (**Fig. 7B)**. Furthermore, the LPS injection

individuals seemed to have weaker correlation than within the control injection group, suggesting a higher variability in gene expression following the immunological stress. A heatmap was performed based on the expression level of DEGs: the result of the clustering found individual replicates of the same condition gathered and split the unigenes into two clear clusters corresponding to up and down-regulated unigenes (**Fig. 7C**). The number of DEGs 24 hours after an LPS challenge seemed to be variable across sea cucumber species with 1,347 DEGs in *A. japonicus* (890 up-regulated and 447 down-regulated; [14]), 7,074 in *H. leucospilota* (666 up-regulated and 6,408 down-regulated; [29]) and 5,524 in *H. forskali* (2,702 up-regulated and 2,822 down-regulated; unpublished data). With 945 DEGs, *H. scabra* appears therefore to display the lower number of DEGs among the sea cucumber species investigated but is the one that shows the maximum ratio of up-regulated/down-regulated genes, namely 2.47. However, it should be noted that the protocol used in the different species was not the same, which could also explain some of the variability in the number of DEGs between species. The full list of DEGs in *H. scabra* can be consulted in **Supplementary Material 4**.

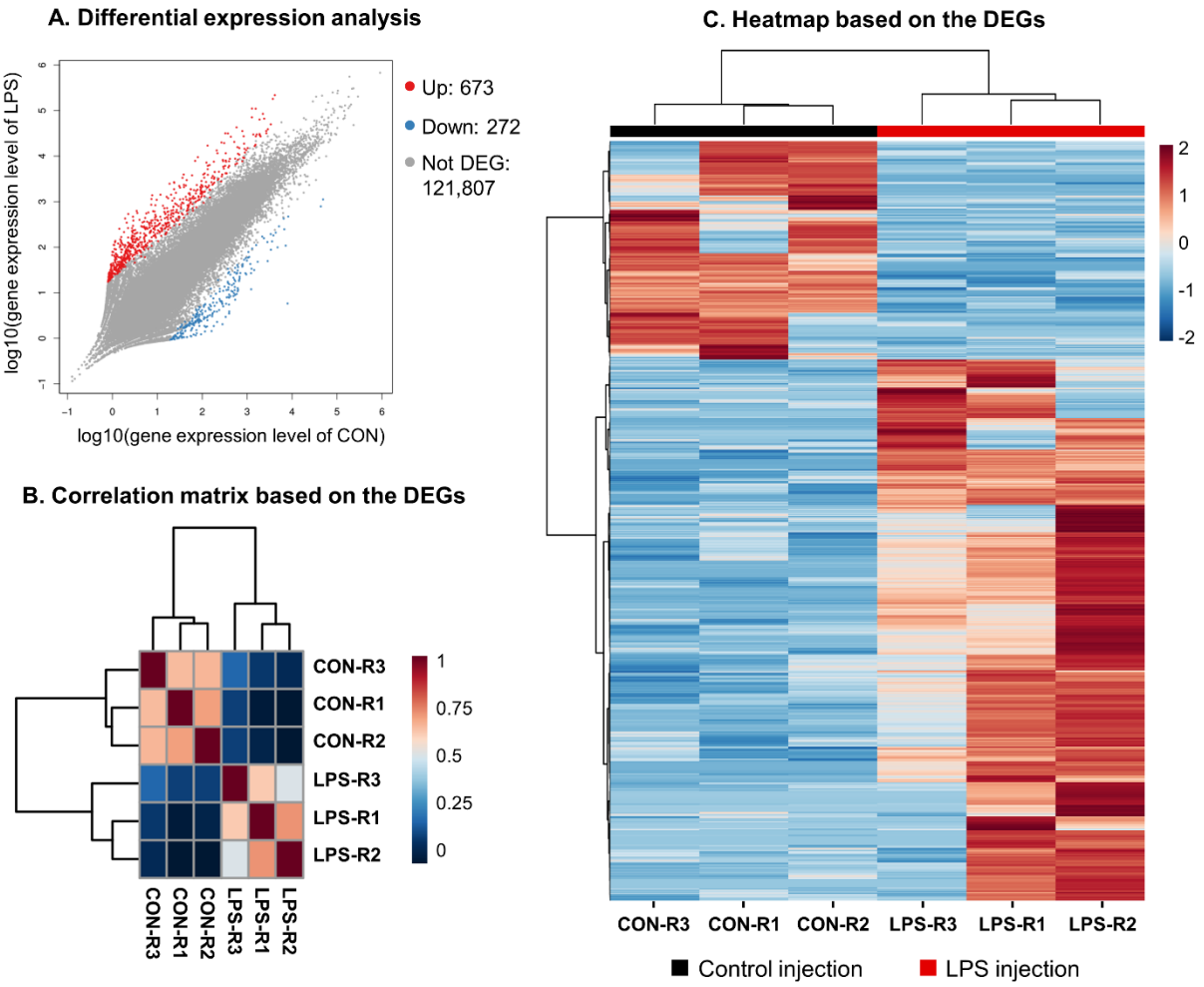

718

719 **Fig. 7.** Differential expression analysis between control and LPS injection individuals
720 in *Holothuria scabra*. A. Scatter plot representation of the differential expression
721 analysis: out of the 122,752 unigenes, 673 were up-regulated (in red; FDR ≤ 5% and
722 $\log_2$ fold change ≥ 1) and 272 were down-regulated (in blue; FDR ≤ 5% and $\log_2$ fold
723 change ≤ -1); the remaining 121,807 were not differentially expressed (in grey; FDR >
724 5% or/and $|\log_2$ fold change$|$ < 1). B. Correlation matrix of the individual replicates
725 based on the 945 DEGs. C. Heatmap based on the 945 DEGs: individuals from the
726 same condition are gathered and DEGs are divided into two clusters corresponding to
727 down-regulated unigenes (above) and up-regulated unigenes (below).

728 *3.2.2.4. Functional distribution and*

729 *enrichment analysis of GO terms and KEGG pathways*

730 Firstly, regarding GO annotations, 160 DEGs were annotated with at least one GO
731 term (16.9%), corresponding to a total of 777 annotations. Among these GO
732 annotations, 325 fell in the category of cellular component, followed by the categories
733 biological process with 251 annotations and molecular function with 201 annotations.

734 Among the most interesting gene ontology related to the immune response, the GO
735 terms “binding” and “catalytic activity” showed 80 and 62 annotations, respectively.

736 Secondly, regarding KEGG annotations, 363 DEGs matched to at least one pathway
737 (38.4%) corresponding to 1073 pathway annotations that were distributed in the
738 following decreasing order: 336 in human diseases; 263 in organismal systems; 160
739 in environmental information processing; 146 in metabolism; 126 in cellular process;
740 and 42 in genetic information processing. Among the organismal system categories,
741 the immune system was the most annotated pathway with 64 annotations. The top ten
742 most enriched pathways are shown in **Table 5**: pertussis pathway was the first followed
743 by protein digestion and absorption and legionellosis. Several infectious human
744 disease pathways are represented which is probably explained by many homologies
745 with proteins of the signalling pathways in response to infection. Cytokine-cytokine
746 receptor interaction pathway can also be highlighted; cytokines are known to play a
747 critical function in inflammation and communication between immune cells [30].
748 Thanks to the KEGG enrichment analysis, we also listed the ten most enriched
749 pathways within the immune system pathways to identify some important pathways
750 involved in the response to LPS injection. The three most enriched immune pathways
751 were Th17 cell differentiation, NOD-like receptor signalling pathways and IL-17
752 signalling pathway (**Table 5**). These three pathways are important in immunity: Th17
753 cells are a subset of T helper pro-inflammatory cells, and their differentiation is
754 mediated by various cytokines [31] that could have some homologues in sea
755 cucumbers; NOD-like receptors are important pathogen recognition receptors [32] and
756 IL-17 is a cytokine involved in the recruitment of immune cells [31]. Other interesting
757 pathways related to immune response were present such as complement and
758 coagulation cascades, Toll and Imd signalling pathway, and Toll-like receptor signalling

pathway. The complement is an important complex of humoral factors that are involved in numerous immune mechanisms including the opsonisation and the stimulation of the adaptive immune system [4]. Toll-like receptors and Imd signalling cascade participate in the recognition and initiation of the immune response in innate immunity [30]. The detailed results of the GO and KEGG functional enrichment can be consulted in **Supplementary Material 5**.

Table 5. KEGG functional enrichment analysis: the 10 most enriched pathways in all pathways (A) and immune system pathways (B). The columns "Annotated DEGs" and "Annotated unigenes" represent the number of unigenes (and proportion) that matched the pathway among the lists of DEGs and all the unigenes, respectively.

	Pathway ID	Annotated DEG	Annotated unigene	P-value	Pathway
			A. All pathways		
1.	**ko05133**	21 (5.79%)	386 (1.31%)	1.72×10^{-8}	Pertussis
2.	**ko04974**	20 (5.51%)	452 (1.53%)	1.02×10^{-6}	Protein digestion and absorption
3.	**ko05134**	16 (4.41%)	340 (1.15%)	5.72×10^{-6}	Legionellosis
4.	**ko05132**	18 (4.96%)	455 (1.54%)	1.62×10^{-5}	Salmonella infection
5.	**ko05164**	21 (5.79%)	599 (2.03%)	2.00×10^{-5}	Influenza A
6.	**ko05200**	43 (11.85%)	1833 (6.21%)	3.85×10^{-5}	Pathways in cancer
7.	**ko04060**	9 (2.48%)	139 (0.47%)	5.87×10^{-5}	Cytokine-cytokine receptor interaction
8.	**ko04510**	29 (7.99%)	1158 (3.92%)	2.58×10^{-4}	Focal adhesion
9.	**ko04972**	13 (3.58%)	343 (1.16%)	3.63×10^{-4}	Pancreatic secretion
10.	**ko04659**	8 (2.2%)	142 (0.48%)	3.89×10^{-4}	Th17 cell differentiation
			B. Immune system pathways		
1.	**ko04659**	8 (2.2%)	142 (0.48%)	3.89×10^{-4}	Th17 cell differentiation
2.	**ko04621**	19 (5.23%)	799 (2.71%)	5.09×10^{-3}	NOD-like receptor signaling pathway
3.	**ko04657**	9 (2.48%)	281 (0.95%)	8.37×10^{-3}	IL-17 signaling pathway
4.	**ko04624**	8 (2.2%)	256 (0.87%)	1.44×10^{-2}	Toll and Imd signaling pathway
5.	**ko04610**	6 (1.65%)	177 (0.6%)	2.26×10^{-2}	Complement and coagulation cascades
6.	**ko04611**	10 (2.75%)	476 (1.61%)	7.13×10^{-2}	Platelet activation

7.	**ko04670**	8 (2.2%)	387 (1.31%)	0.106	Leukocyte transendothelial migration
8.	**ko04612**	3 (0.83%)	107 (0.36%)	0.145	Antigen processing and presentation
9.	**ko04658**	10 (2.75%)	583 (1.98%)	0.183	Th1 and Th2 cell differentiation
10.	**ko04620**	4 (1.1%)	246 (0.83%)	0.358	Toll-like receptor signaling pathway

3.2.2.5. Identification of immune differentially expressed unigenes

A total of 80 immune differentially expressed genes (IDEGs) were identified based on KEGG enrichment analysis and keyword research, of which 52 were up-regulated and 28 were down-regulated in LPS injection individuals. Among the 64 unigenes that were classified in the general pathway “immune system”, 41 were selected based on their relevance to their immune function(s) (64%). The remaining 39 IDEGs were selected by the keyword research based on their annotation that matched immune genes of interest reported in previous studies about echinoderm immunity [4,16,17]. IDEGs were classified into 17 “gene families” that were defined based on presumed immune functions or existing protein families to enhance the readability of the IDEGs list. This list is shown in **Figures 8 and 9** and the full list containing all the unigenes annotated in the immune system pathway, as well as unigenes selected by keyword search, can be consulted in **Supplementary Material 6**.

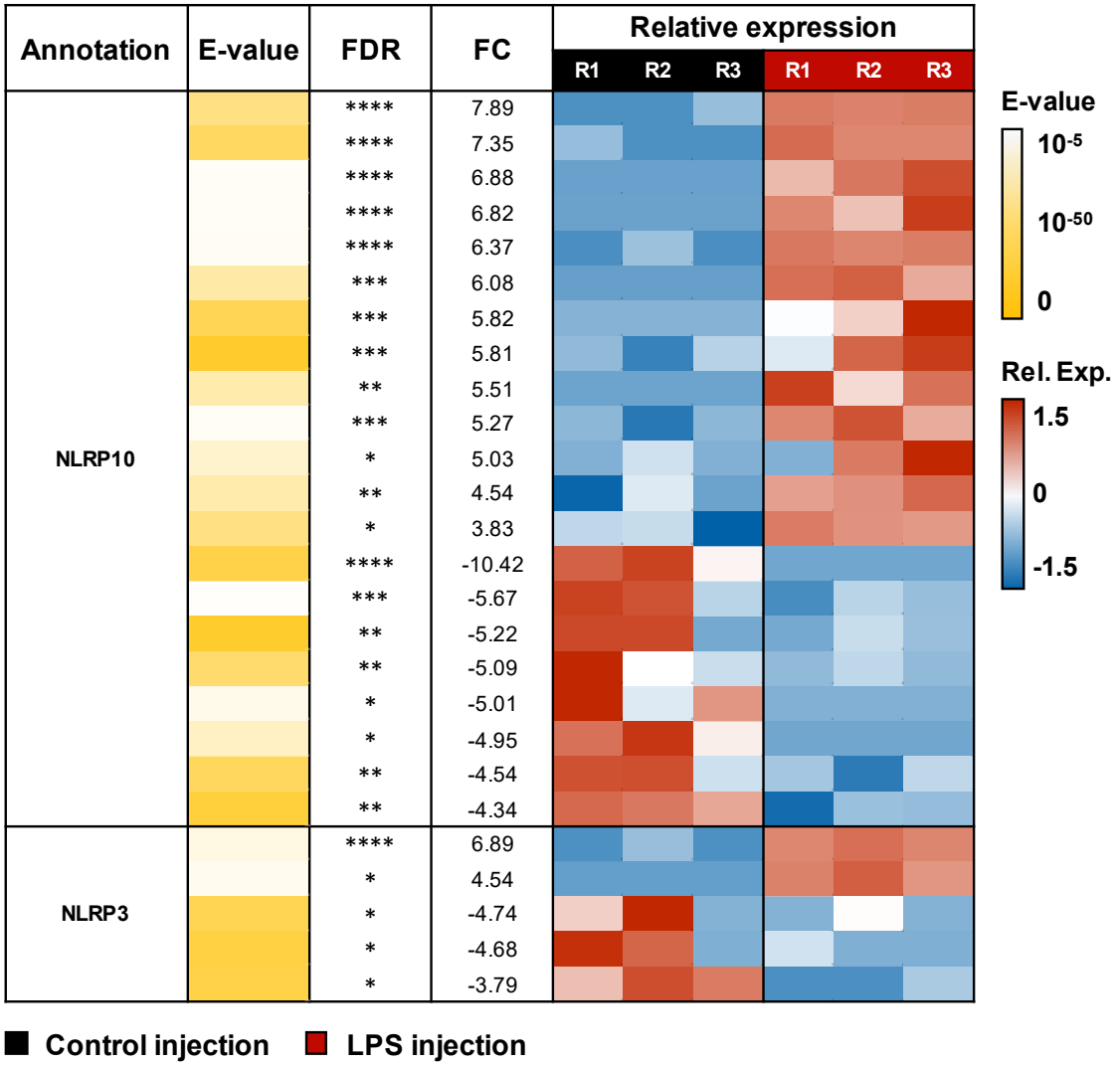

784

785 **Fig. 8.** List of immune differentially expressed unigenes (IDEGs) in the "gene family"
786 of NLRPs (see explanations in the text). For each unigene is provided: the functional
787 annotation (when possible as an abbreviation, the full name is visible in the text or
788 **Supplementary Material 6**); the associated E-value as a colour scale; the false
789 discovery rate (* FDR ≤ 5%; ** FDR ≤ 1%; *** FDR ≤ 0.1%; **** FDR ≤ 0.01%); the FC
790 value (formulated as $\log_2$(FC): a positive FC means up-regulated and negative FC
791 means down-regulated in LPS injection individuals); the relative expression for each
792 replicate (FPKM transformed by $\log_{10}$ and autoscaled). Among the same gene family,
793 unigenes are ordered from the highest to the lowest FC for up-regulated unigenes, and
794 then from the lowest to the highest for down-regulated unigenes. Legend: FC – fold
795 change; FDR – false discovery rate; LPS injection – lipopolysaccharide injection
796 individuals; R – individual replicate; Rel. Exp. – relative expression.

Gene Family	Annotation	E-value	FDR	FC	Relative expression					
					R1	R2	R3	R1	R2	R3
Cytokines and related proteins	Interleukin-17-5		***	6.22						
	IRAK4		***	5.81						
	IFN-induce GTPase 1-like iso. X2		**	5.39						
	Putative interleukin 17-like protein		*	4.70						
	Interleukin-25		**	4.55						
	Interleukin 17-like protein		*	4.12						
	IL1RAP		*	4.02						
	ADAMTS		*	4.01						
	ADAMTS		*	3.75						
	IFN-induce GTPase 1-like		***	-5.83						
Lectins	Lactose-binding lectin I-2 iso. X2		***	5.94						
	C-type lectin d.-c. protein 162		**	5.47						
	Techylectin-5A-like iso. X2		**	4.91						
	Ladderlectin-like		**	4.71						
	Techylectin-5B		**	-5.06						
	Techylectin-5B		**	-4.94						
SVEP1	SVEP1		****	6.89						
	SVEP1 iso. X2		****	6.40						
	SVEP1 iso. X2		****	6.21						
	SVEP1 iso. X2		****	5.99						
	SVEP1		***	5.94						
	SVEP1		***	5.53						
Apoptosis	TNIP3		**	4.69						
	TNIP3		*	3.89						
	SH3BGRL3		**	-5.58						
	FADD protein		*	-4.88						
	BOK		*	-4.08						
Coagulation	Amassin-2 precursor		***	5.07						
	Amassin-2 precursor		***	4.79						
	Coagulation factor VII		***	-5.71						
	Arylsulfatase E		**	-5.04						
	Arylsulfatase B iso. X3		*	-4.46						
Complement	MRC2-like iso. X2		**	4.88						
	MRC2-like iso. X3		*	4.73						
	Complement factor B		*	4.44						
	MMR1-like		*	4.36						
	Ficolin-2-like		**	-5.19						
Integrins	Integrin beta-1-B-like		**	-5.51						
	Integrin beta-1-A		*	-4.45						
	Integrin beta-1-B-like		*	-4.37						
	Integrin beta-1-B-like		*	-3.91						
Heat shock proteins	HSP70		**	5.27						
	HSP26		*	4.86						
	HSP70		*	4.44						
	HSP26		*	4.13						
Antioxidant	PHGPx		*	3.87						
	Glutathione peroxidase		*	3.66						
Epidermal growth factors	Fibropellin-3 iso. X3		*	3.99						
	Fibropellin-3-like		*	-4.37						
Ca^{2+} regulation	CD38-like		****	7.49						
Lysin	Lysozyme		*	-4.89						
Phenoloxidase	Laccase-type phenoloxidase		*	3.51						
SCRC	DMBT1-like		*	4.57						
Tetraspanin	CD63 antigen-like		**	-5.26						

■ Control injection ■ LPS injection

Fig. 9. List of immune differentially expressed unigenes (IDEGs). For each unigene is provided: the "gene family"; the functional annotation (when possible as an abbreviation, the full name is visible in the text or **Supplementary Material 6**); the associated E-value as a colour scale; the false discovery rate (* FDR ≤ 5%; ** FDR ≤ 1%; *** FDR ≤ 0.1%; **** FDR ≤ 0.01%); the FC value (formulated as $\log_2$(FC): a positive FC means up-regulated and a negative FC means down-regulated in LPS

injection individuals); the relative expression for each replicate (FPKM transformed by log_{10} and autoscaled). Among the same gene family, unigenes are ordered from the highest to the lowest FC for up-regulated unigenes, and then from the lowest to the highest for down-regulated unigenes. Legend: d.-c. – domain-containing; FC – fold change; FDR – false discovery rate; iso. – isoform; LPS injection – lipopolysaccharide injection individual; R – individual replicate; Rel. Exp. – relative expression.

The most represented gene family among IDEGs was NLRPs (Nucleotide-binding oligomerization domain, Leucine-rich Repeat and Pyrin domain-containing) with a total of 26 unigenes (**Fig. 8**). Of these, 21 were annotated as NLRP10 and 5 as NLRP3 both in *A. japonicus*. Surprisingly, unigenes that shared the same annotation could be up-regulated or down-regulated: for unigenes annotated as NLRP10, 13 were up-regulated (61.9%) and 8 were down-regulated (38.1%) and for unigenes annotated as NLRP3, 2 were up-regulated (40%) and 3 were down-regulated (60%). It should also be noted that the transcriptome contains 274 unigenes annotated as NLRP10 and 86 annotated as NLRP3 that were not differentially expressed. Therefore, 7.1% of unigenes annotated as NLRP10 and 5.5% of unigenes annotated as NLRP3 were differentially expressed. NLRP are members of the NLR family (NOD-like receptors), one of the main categories of pathogen recognition receptors (PRRs), which are known to play an important function in the innate immune system by regulating the inflammation process, promoting the mature form of the cytokines IL-1β and IL-18 and inducing a particular type of programmed cell death called pyroptosis [31]. In the sea cucumber *A. japonicus*, it was demonstrated that both NLRP10 and NLRP3 are involved in the response of bacterial infection: NLRP10 decrease the level of Caspase-1 and MMP37, inhibiting the pyroptosis [33] whereas NLRP3 promotes the inflammation in the same way as described in vertebrates [34]. The large number of unigenes annotated as NLRPs in *H. scabra* may be explained by an expansion of the genes encoding these receptors, as was demonstrated for several immune gene families in the sea urchin genome [17]. To elucidate the origin of this diversity, it would

be useful to carry out more in-depth sequence analyses using genomic data from diverse sea cucumber species (see also section 3.2.5.).

The gene family that comes next is cytokines and related proteins, with a total of ten unigenes (**Fig. 9**). Among these, three were annotated as interleukin 17 (interleukin-17-5, interleukin 17-like protein, putative interleukin 17-like protein), two as interferon-induce GTPase 1-like (IFN-induce GTPase 1-like), one as interleukin-1 receptor-associated kinase 4 (IRAK4), one as interleukin 25, one as interleukin-1 receptor accessory protein (IL1RAP) and two as a disintegrin and metalloproteinase with thrombospondin motifs (ADAMTS). All were up-regulated in the LPS injection group except one of the unigenes annotated as IFN-induce GTPase 1-like. Cytokines are important immune proteins that stimulate inflammation and participate in the recruitment of immune cells [30,31]. In sea cucumbers, Wu et al. [29] reported four families of cytokines including BCL/CLL, EPRF1, IL-17 and TSP/TPO among whichIL-17 was the most expressed family 24 hours after an exposition to LPS in the species *H. leucospilota.* In our study, mainly IL-17 family members were identified although two unigenes annotated as ADAMTS thrombospondin-containing motifs (as in TSP/TPO in [29]) and one as BOK, a member of BCL/CLL family (classified in apoptosis gene family in **Fig. 9**). Therefore, our results corroborate the result obtained in *H. leucospilota* which suggest that IL-17 cytokines are the most important cytokine family in the holothuroid immune response to bacterial infection.

Among IDEGs, six lectins were identified including one lactose-binding lectin, one C-type lectin domain-containing protein 162, one ladderlectin-like and three techylectin-like. Most were up-regulated except two techylectin-like (**Fig. 9**). Lectins are PRRs specialised in the recognition of sugar motifs [4]. In *H. scabra*, a T-antigen-specific lectin was purified from the PF and its agglutinin and antibacterial activity was

857 demonstrated against both Gram-negative and Gram-positive bacteria [35]. More
858 recently, it was shown that C-type lectins have also an important function in host
859 defence and that their activity is calcium-dependent in *A. japonicus* [36]. Our results
860 support that lectins are an important component of the innate immune response in sea
861 cucumbers and suggest that a large diversity of lectin types is involved in this response.

862 Six DEGs were annotated as sushi, von Willebrand factor type A, EGF and pentraxin
863 domain-containing protein 1-like (SVEP1-like) and all were up-regulated (**Fig. 9.**).
864 SVEP1 is an extracellular matrix protein that contains several domains including a
865 pentraxin domain [37]. Pentraxins are highly conserved domains that act as PRRs and
866 are involved in the acute innate immune response. More specifically, SVEP1 is mainly
867 known in humans to promote vascular disease because of its interaction with platelet
868 receptors [37]. In sea cucumbers, the overexpression of SVEP1-like suggests that
869 these genes could be involved in the recognition of Gram-negative bacteria and could
870 also act as an agglutinin.

871 Then, five DEGs were presumed to have a function in apoptosis (**Fig. 9**). These
872 comprise two unigenes annotated as tumour necrosis factor-α induced protein 3
873 interacting protein 3-like (TNFAIP3 interacting protein or TNIP3-like) [38], one
874 annotated as SH3 domain-binding glutamic acid-rich-like protein 3 (SH3BGRL3) [39],
875 one annotated as FAS-associated death domain protein (FADD protein) [40], and one
876 annotated as BCL-2-related ovarian killer protein (BOK) [41]. While unigenes
877 annotated as TNIP3 were up-regulated, other unigenes involved in apoptosis were
878 down-regulated. The differential expression of all these unigenes shows contradicting
879 effects (*i.e.* activation and inhibition of apoptosis at the same time) suggesting a fine
880 regulation of apoptosis 24 hours after the LPS injection in *H. scabra*.

Five DEGs were identified to participate in the coagulation processes, namely two unigenes annotated as amassin-2 precursor, two unigenes annotated as arylsulfatase (E and B) and one unigene annotated as coagulation factor VII (**Fig. 9**). Amassin is a secreted plasmatic protein that was first identified in sea urchins to play a critical function in cœlomocyte aggregation by forming extracellular bridges of disulphide bonds between cells when polymerising [42]. However, the protein linking the cells to the amassin complex was not identified. Later, D'Andrea-Winslow et al. [43] demonstrated the importance of arylsulfatase in clotting and proposed that this protein could be the extracellular membrane protein responsible for this link between cœlomocyte and amassin bridges. While amassin-precursors are strongly up-regulated in our results, arylsulfatase E and B are down-regulated, casting doubt on this hypothesis of a possible interaction or at least suggesting that these two genes are not necessarily co-expressed. Regarding the unigene annotated as coagulation factor VII, in contrast to the majority of other unigenes that matched genes from echinoderm genomes, the unigenes coding for the coagulation factor VII matched the genome of *Mus musculus* (see complete annotations in **Supplementary Material 6**). In vertebrates, this particular serine protease has a critical function in coagulation by initiating the coagulation cascade when encountering tissue damage [44]. In echinoderms; it was only shown that a low-density lipoprotein-receptor-related protein 4 precursor of the genome of the sea urchin *Strongylocentrotus purpuratus* shared 34% of identity with serine protease sequences in humans [43]. In our results, while Nr annotation results in “low-density lipoprotein receptor-related protein 4-like [*Acanthaster planci*]” (E-value = 5.5×10^{-51}), SwissProt annotation results in “Coagulation factor VII OS=*Mus musculus* GN=F7 PE=1 SV=1” (E-value = 5.2×10^{-43}), suggesting that the genome of *H. scabra* share the same identity with coagulation

906 factor VII as *S. purpuratus*. In addition, serine proteases are known to participate in an
907 enzymatic cascade that leads to the maturation of prophenoloxidase into active
908 phenoloxidase in arthropods, the enzyme responsible for melanisation [25]. Here,
909 more than highlighting its presence in the transcriptome of *H. scabra*, we have shown
910 that this unigene is down-regulated after the LPS injection, which was also
911 demonstrated by cDNA amplification (see 3.2.2.6.), suggesting it could have a function
912 in the response to immunological stress in echinoderms as well.

913 Five DEGs were identified for their involvement in the complement system [14]. They
914 include two unigenes annotated as C-type mannose receptor 2-like (MRC2-like), one
915 annotated as complement factor B, one as macrophage mannose receptor 1-like
916 (MMR1-like), and one annotated as ficolin-2-like (**Fig. 9**). In vertebrates, activation of
917 this system leads to various immune mechanisms including phagocytosis, lysis and
918 inflammation [4]. The study by Dong et al. [12] showed that in *A. japonicus*,
919 immunostimulation with LPS led to the overexpression of factor C3 and factor B in
920 cœlomocytes. In our study, while unigenes annotated as factor B and as mannose-
921 binding receptors were overexpressed, unigenes annotated as ficolin-2 homologue
922 were underexpressed after injection of LPS. These results suggest a potential
923 activation of the complement system by the lectin-type activation pathway and more
924 specifically by that involving mannose receptors in the presence of LPS. However, it
925 should be noted that in the transcriptome of *H. scabra*, five unigenes were annotated
926 as complement component C3 in *A. japonicus*, but all these unigenes were not
927 differentially expressed (FDR > 5% or/and $|\log_2 \text{fold change}| < 1$).

928 The next gene family was integrin with three DEGs annotated as integrin beta-1-B and
929 one annotated as integrin beta-1-A (**Fig. 9**). The four unigenes were down-regulated
930 following the LPS injection. In sea cucumbers, Wang et al. [45] demonstrated that β-

integrin was down-regulated in cœlomocytes after an LPS challenge. Interestingly, silencing β-integrin promotes cœlomocyte apoptosis. Our results corroborate those obtained by Wang et al. [45]; the underexpression of integrin beta-1-B and A in *H. scabra* suggests that apoptosis was promoted by this pathway 24 hours after the injection of LPS.

Four unigenes annotated as heat shock protein (HSP) were up-regulated and comprised two unigenes annotated as HSP70 and two others annotated as HSP26 (**Fig. 9**). HSP family members are highly conserved proteins which have the function of chaperones, *i.e.* they help other proteins to acquire a proper conformation [46]. It was also reported that some HSPs such as HSP70 can act as an activator of the innate immune system by playing the function of danger-signalling molecules [46]. In sea cucumbers, the overexpression of HSPs was shown in various contexts of stress including thermal stress [47] and exposition to pathogens [12].Our results confirm that they are involved in the response to immunological stress.

Then, two DEGs coding for proteins having an antioxidant activity were identified, they were annotated as phospholipid hydroperoxide glutathione peroxidase (PHGPx) and glutathione peroxidase (GPx) [48], and both were up-regulated following the LPS injection (**Fig. 9**). The overexpression of PHGPx and GPx under immunological stress in *H. scabra* could be a regulation process after the release of reactive oxygen species (ROS) during the acute immune response. This function of GPx is for example known to occur after the melanisation process in arthropods [24].

Two DEGs were annotated as fibropellin 3 (fibropellin 3 and fibropellin 3-like), of which one was up-regulated and the other was down-regulated (**Fig. 9**). Fibropellins are a family of extracellular matrix proteins that contain repeated epidermal growth factor-

like motifs. It was first described as constituting the apical lamina of sea urchin embryos [49]. In the sea cucumber *A. japonicus*, fibropellin was later reported to have a function in regeneration, notably after evisceration [49]. Therefore, the differential expression of fibropellin could suggest that immunological stress can involve mechanisms of tissue regeneration in *H. scabra*.

Finally, five DEGs have their particular function in the immune response and were classified separately: they comprise ADP-ribosyl cyclase/cyclic ADP-ribose hydrolase 1-like (CD38-like), Lysozyme, Laccase-type phenoloxidase, deleted in malignant brain tumours 1 protein-like (DMBT1-like), and tetraspanin (CD63-like) (**Fig. 9**). CD38 is a transmembrane protein that, upon interaction with the proper ligand, can mobilise the intracellular reserve of calcium cations (Ca^{2+}) [50]. Divalent cations such as Ca^{2+} and Mg^{2+} are important mediators of the immune response and regulate a large spectrum of mechanisms including aggregation and inflammation [13,42]. CD38-like was up-regulated following the LPS injection which can be attributed to the Ca^{2+} release as a signal to stimulate the immune response in *H. scabra*. The DEG annotated as lysozyme was surprisingly underexpressed in the LPS injection group. These proteins are lysins, humoral factors that possess a lytic activity) [29]. They are particularly active against Gram-positive bacteria because these bacteria do not have an outer membrane containing LPS, unlike Gram-negative bacteria[29]. We could therefore hypothesise that the presence of LPS, mimicking the presence of Gram-negative bacteria, does not lead to greater production of lysozyme.

The DEG annotated as laccase-type phenoloxidase was overexpressed in the LPS injection group. The phenoloxidase constitutes the key component of the melanisation cascade in many taxa [51]. In the sea cucumber *A. japonicus*, it was shown that the expression of a laccase-type phenoloxidase was the highest in cœlomocytes

compared to other tissues, and was enhanced under immunostimulation with LPS, peptidoglycans and Zymosan A and PolyI:C; and was maximal 24 hours after the exposition to these different immunostimulants, except for peptidoglycans for which the peak occur 12 hours after the immunostimulation [52]. Therefore, our results strongly corroborate the results obtained in *A. japonicus*.

The DEG annotated as DMBT1-like was overexpressed in the LPS injection group. DMBT1 is a glycoprotein that contains multiple scavenger receptor cysteine-rich (SRCR) domains, which are known to have a function of PRRs [11]. In *A. japonicus*, it was shown that DMBT1-like was up-regulated 24 hours after an immunostimulation with *V. splendidus* in the cœlomocytes from the PF but not in cœlomocytes from the HF [11,53]. These results are consistent with those found in *H. scabra* and suggest that DMBT1-like is an important PRR of Gram-negative bacteria or LPS.

The DEG annotated as CD63 antigen-like was down-regulated in the LPS injection group. CD63 is a transmembrane protein participating in a large spectrum of cellular mechanisms including cell activation, cell adhesion and cell differentiation [54]. While the functions ofCD63 in the immune response have never been demonstrated yet in an echinoderm, in oyster *Crassostrea gigas* it was shown that it could have a role of pathogen receptor that promotes phagocytosis, notably by binding lipopolysaccharides [54].

had an effect to activate hemocytes (*i.e.* equivalent of coelomocytes in arthropods)[54].

3.2.2.6. Validation of differential gene expression

To validate the differential expression analysis obtained by RNA-seq, an independent experiment was achieved to quantify the expression of a selection of immune genes (**Fig. 10. A and B**). Overall, results show a significant relation between the two

techniques (R^2 = 0.71; P = 3.6 × 10^{-2}; F = 9.646; DFn = 1; DFd = 4). However, it should be highlighted that while some genes strongly corroborate the results obtained by the RNA-seq (*e.g.* Coagulation factor VII, Interleukin 17-like protein and laccase-type phenoloxidase), others had a highly variable expression within the two conditions (*e.g.* the two NLRP10 and ADAMTS), suggesting a complex regulation of these genes which is consistent with results obtained for NLRP genes in the RNA-seq data. Gel electrophoresis results are shown in **Supplementary Material 7**.

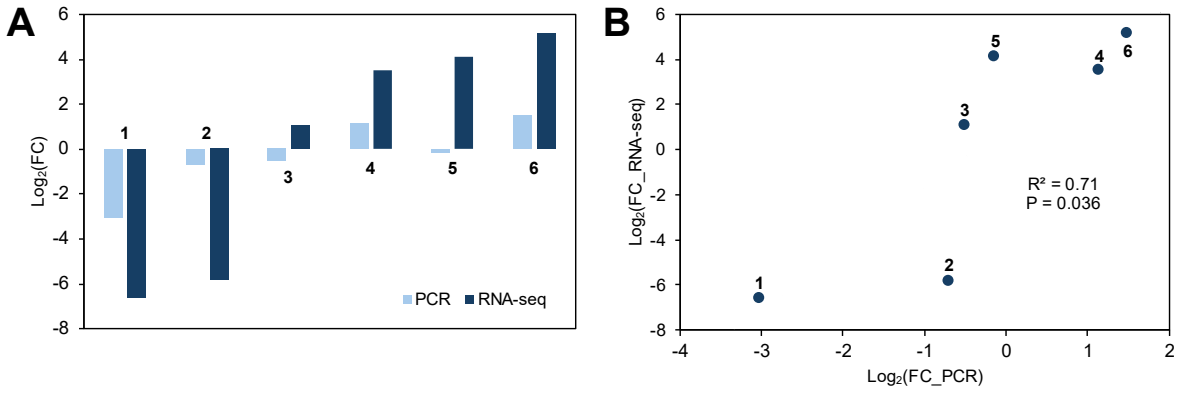

Fig. 10. Validation of the RNA-seq differential expression analysis using visualisation of amplified cDNA on electrophoresis gel. Electrophoresis gel of each gene can be consulted in **Supplementary Material 7** including a control gel carried with 16S RNA showing an equivalent expression between control and LPS-injected individuals. A. Comparison of the fold change (FC) value between RNA-seq and PCR results (n = 5 per condition). B. Linear regression between PCR and RNA-sequencing results showing a significant relation (R^2 – coefficient of determination; P – F-test p-value).

3.2.3. Relation between cœlomocyte populations and gene expression

Studies of gene expression in holothuroids often considered cœlomocytes as an entity, neglecting the cell type heterogeneity that constitutes this pool of cells (*e.g.* [11,12,28]). In this way, the differential gene expression is generally considered as the result of an expression shift in cœlomocytes but could also be the result of a shift in cell populations

with a stable gene expression. Both effects probably influence gene expression results, but the gene expression and cell population modification are rarely assessed at the same time. Recently, it was shown that cœlomocytes from the PF and the HF of *A. japonicus* have a divergent expression of some immune genes, the two fluids having different proportions in cell populations [53]. Furthermore, Yu et al. [55] demonstrated that two subsets of cells from the PF, namely spherical cells and lymphocyte-like cells, had their own gene expression profile. These two examples prove that assessing the change in cell populations is crucial for interpreting the transcriptomics analysis as well as other types of omics analyses.

Here, the transcriptomic analysis focused on the comparison between control injection and LPS injection individuals to avoid an “injection stress effect”. Despite high inter-individual variability, the proportions of coelomocyte populations were similar between these two conditions compared with the non-injected group. This suggests therefore that the variability in gene expression is mainly due to a shift in gene expression rather than a shift in cell populations. Unfortunately, it was not possible to estimate directly the proportion of the different coelomocyte populations in the sequenced samples due to logistical limitations related to the fieldwork in Madagascar, but it would be interesting to take this into account in future analyses.

3.2.4. Inter-individual variability in the immune response *H. scabra*

Overall, our results showed particularly high inter-individual variability, especially for cell concentration and proportions. This high variability can be explained by several factors including the sex, the age, and the life story of the animal. Unfortunately, it was impossible to determine the sex in our experiment. Regarding the age and the life history, although these phenotypic factors cannot be totally under control, specimens of *H. scabra* used for the experimentations came from the same aquaculture pens and

were born in the same hatcheries. Over their growth, they followed the same rearing process and were divided into different enclosures as a function of their size. Therefore, we could expect that individuals collected from the same sea pen were similarly aged. Finally, the high inter-individual variability encountered in *H. scabra* is not an exception and was observed in other sea cucumber species (*e.g. H. poli* [20], *A. japonicus* [19], *C. frondosa* [5]) as well as in other echinoderm classes (*e.g. Paracentrotus lividus* [26]). This variability suggests a highly reactive immune system implicating complex regulatory systems in echinoderms.

3.2.5. New insights into the holothuroid immune system

While most of the immune genes presented in this study have already been identified in other echinoderm species, particularly in the extensively studied sea cucumber *A. japonicus*, this immune gene repertoire offers valuable insights into comparative immunology. In addition, our research also uncovered genes that have not been previously considered in echinoderm immunology but may exhibit immune-related functions based on the functions of orthologs in other phyla. Examples include coagulation factor VII and CD63 antigen-like that have specific immune-related functions in vertebrates and molluscs, respectively [44, 54]. These genes warrant targeted functional analyses to establish their significance in sea cucumber immune response.

Our study also emphasizes the extensive diversity of reconstructed transcripts associated with a single annotation, with distinct transcripts exhibiting widely varying expression levels (*e.g.* NLRPs, lectins, fibropellins). While these observations are challenging to interpret and may, to some extent, result from artefacts of *de novo* transcriptome reconstruction, the phenomenon is particularly pronounced in the NLR family. This gene family appears to play a crucial role in the bacterial response of *H.*

scabra, as evidenced by the high number of DEGs it encompasses. Interestingly, it was recently shown in sea urchins that distinct coelomocyte subpopulations obtained from the same individual can have distinct genomic variants for the same gene family, such as the SpTransformer genes [56]. It is important to note that the concept of somatic gene diversification, particularly in the case of SpTransformer genes, has been called into question and potentially attributed, at least in part, to experimental biases [57]. To the best of our knowledge, this work has not yet been published in a peer-reviewed journal, leaving the question unresolved within the scientific community. While the mechanisms underlying this genomic diversity remain elusive, the resulting variation enhances the functional diversity of pathogen recognition receptors in this group [57]. Regarding NLRs, prior studies on *A. japonicus* have revealed that a specific NLRC4-type gene (another gene in the NLR family) possesses a unique structure that includes an immunoglobulin domain [58]. Such domains are known to be particularly prone to alternative splicing, a process that could diversify protein structures, as observed in the Dscam protein of the Chinese mitten crab [59]. Our preliminary data suggest that several NLRP10 variants identified in this study share structural similarities with AjNLRC4 (unpublished data). Ongoing research aims to further characterize the diversity of these NLRs in sea cucumbers, investigate mechanisms underlying their functional diversification, and determine whether these NLRs, and their associated high diversity, represent a distinctive feature of the sea cucumber immune system.

4. Conclusion

This study describes the different molecular and cellular components of the immune system in the aquacultivated and endangered species *H. scabra*. Five main cell types were described in the HF and PF including, in order of decreasing proportion, phagocytes, SRCs, spherulocytes, fusiform cells and crystal cells. No clear relation was found in the cell population between the two fluids. The injection of LPS and sterile seawater showed mainly a tendency of a decrease in phagocyte proportion concomitant with an increase of SRC proportion in both fluids, which would be explained by the recruitment of stem cells to replace the utilisation of immune active cells. Finally, the gene expression analysis of cœlomocytes from the PF 24 hours following LPS injections showed the differential expression of a large number of genes involved in highly diverse immune mechanisms.

All these results emphasise the high complexity of the immune system in *H. scabra* and will be useful to better understand its biology in the context of aquaculture as well as provide interesting data for comparative immunology.

5. Acknowledgements

Firstly, we acknowledge the *Institut Halieutique et des Sciences Marines* (IH.SM) of Toliara for the logistical support, especially the technician Hanitriniala Mahavory for her availability. We also thank Indian Ocean Trepang for allowing us to collect sea cucumbers in their offshore facilities, with special thanks to Loïc Gaumez for his precious help during the fieldwork. We are grateful to Mabel Castiaux, who was also a great help during the fieldwork. Finally, we thank an anonymous reviewer for his constructive comments. This work was supported by an FRIA F.R.S-FNRS grant to

NW (47487) and the PDR F.R.S-FNRS project “Protectobiome in sea cucumbers” from IE, FB and JD (40013965).

6. Author contributions

Noé Wambreuse: Conceptualisation, Formal analysis, Methodology, Writing the original draft, Writing - review and editing. **Guillaume Caulier:** Conceptualisation, Writing - review and editing, Supervision. **Igor Eeckhaut:** Conceptualisation, Writing - review and editing, Project administration, Funding acquisition, Supervision. **Laura Borrello:** Conceptualisation, Methodology, Formal analysis. **Fabrice Bureau:** Conceptualisation, Writing - review and editing, Project administration, Funding acquisition, Supervision. **Laurence Fievez:** Conceptualisation, Writing - review and editing. **Jérôme Delroisse:** Conceptualisation, Formal analysis, Methodology, Writing - review and editing, Supervision.

7. Declaration of competing interest

The authors declare that they have no known competing financial interests or personal relationships that could influence the work reported in this paper.

8. Data Availability

SRA archive files are publicly accessible via the NCBI SRA servers under the BioProject PRJNA1193643 or at the following link:

https://www.ncbi.nlm.nih.gov/sra/PRJNA1193643.

Other types of data can be provided by the authors under reasonable request.

9. References

[1] S.W. Purcell, Value, Market Preferences and Trade of Beche-De-Mer from Pacific Island Sea Cucumbers, PLoS ONE. 9 (2014) e95075. https://doi.org/10.1371/journal.pone.0095075.

[2] J.-F. Hamel, I. Eeckhaut, C. Conand, J. Sun, G. Caulier, A. Mercier, Global knowledge on the commercial sea cucumber *Holothuria scabra*, in: Adv. Mar. Biol., Elsevier, 2022: pp. 1–286. https://doi.org/10.1016/bs.amb.2022.04.001.

[3] J. Delroisse, K. Van Wayneberghe, P. Flammang, D. Gillan, P. Gerbaux, N. Opina, G.G.B. Todinanahary, I. Eeckhaut, Epidemiology of a SKin Ulceration Disease (SKUD) in the sea cucumber *Holothuria scabra* with a review on the SKUDs in Holothuroidea (Echinodermata), Sci. Rep. 10 (2020) 22150. https://doi.org/10.1038/s41598-020-78876-0.

[4] L.C. Smith, V. Arizza, M.A. Barela Hudgell, G. Barone, A.G. Bodnar, K.M. Buckley, V. Cunsolo, N.M. Dheilly, N. Franchi, S.D. Fugmann, R. Furukawa, J. Garcia-Arraras, J.H. Henson, T. Hibino, Z.H. Irons, C. Li, C.M. Lun, A.J. Majeske, M. Oren, P. Pagliara, A. Pinsino, D.A. Raftos, J.P. Rast, B. Samasa, D. Schillaci, C.S. Schrankel, L. Stabili, K. Stensväg, E. Sutton, Echinodermata: The Complex Immune System in Echinoderms, in: E.L. Cooper (Ed.), Adv. Comp. Immunol., Springer International Publishing, Cham, 2018: pp. 409–501. https://doi.org/10.1007/978-3-319-76768-0_13.

[5] G. Caulier, J.-F. Hamel, A. Mercier, From Coelomocytes to Colored Aggregates: Cellular Components and Processes Involved in the Immune Response of the Holothuroid *Cucumaria frondosa*, Biol. Bull. 239 (2020) 95–114. https://doi.org/10.1086/710355.

[6] M.G. Eliseikina, T.Yu. Magarlamov, Coelomocyte Morphology in the Holothurians *Apostichopus japonicus* (Aspidochirota: Stichopodidae) and *Cucumaria japonica* (Dendrochirota: Cucumariidae), Russ. J. Mar. Biol. 28 (2002) 197–202. https://doi.org/10.1023/A:1016801521216.

[7] K. Xing, H. Yang, M. Chen, Morphological and ultrastructural characterization of the coelomocytes in *Apostichopus japonicus*, Aquat. Biol. 2 (2008) 85–92. https://doi.org/10.3354/ab00038.

[8] H.R. Hetzel, Studies on Holothurian Coelomocytes. I. A Survey of Coelomocyte Types, Biol. Bull. 125 (1963) 289–301. https://doi.org/10.2307/1539404.

[9] Y. Prompoon, W. Weerachatyanukul, B. Withyachumnarnkul, Lectin-Based Profiling of Coelomocytes in *Holothuria scabra* and Expression of Superoxide Dismutase in Purified Coelomocytes, Zoolog. Sci. 32 (2015) 345. https://doi.org/10.2108/zs140285.

[10] R.A. Oomen, J.A. Hutchings, Transcriptomic responses to environmental change in fishes: Insights from RNA sequencing, FACETS. 2 (2017) 610–641. https://doi.org/10.1139/facets-2017-0015.

[11] Q. Gao, M. Liao, Y. Wang, B. Li, Z. Zhang, X. Rong, G. Chen, L. Wang, Transcriptome Analysis and Discovery of Genes Involved in Immune Pathways from Coelomocytes of Sea Cucumber (*Apostichopus japonicus*) after *Vibrio splendidus* Challenge, Int. J. Mol. Sci. 16 (2015) 16347–16377. https://doi.org/10.3390/ijms160716347.

[12] Y. Dong, H. Sun, Z. Zhou, A. Yang, Z. Chen, X. Guan, S. Gao, B. Wang, B. Jiang, J. Jiang, Expression Analysis of Immune Related Genes Identified from the Coelomocytes of Sea Cucumber (*Apostichopus japonicus*) in Response to

LPS Challenge, Int. J. Mol. Sci. 15 (2014) 19472–19486. https://doi.org/10.3390/ijms151119472.
[13] L.C. Smith, T.S. Hawley, J.H. Henson, A.J. Majeske, M. Oren, B. Rosental, Methods for collection, handling, and analysis of sea urchin coelomocytes, in: Methods Cell Biol., Elsevier, 2019: pp. 357–389. https://doi.org/10.1016/bs.mcb.2018.11.009.
[14] Z.C. Zhou, Y. Dong, H.J. Sun, A.F. Yang, Z. Chen, S. Gao, J.W. Jiang, X.Y. Guan, B. Jiang, B. Wang, Transcriptome sequencing of sea cucumber (*Apostichopus japonicus*) and the identification of gene-associated markers, Mol. Ecol. Resour. 14 (2014) 127–138. https://doi.org/10.1111/1755-0998.12147.
[15] F.A. Simão, R.M. Waterhouse, P. Ioannidis, E.V. Kriventseva, E.M. Zdobnov, BUSCO: assessing genome assembly and annotation completeness with single-copy orthologs, Bioinformatics. 31 (2015) 3210–3212. https://doi.org/10.1093/bioinformatics/btv351.
[16] Z. Xue, H. Li, X. Wang, X. Li, Y. Liu, J. Sun, C. Liu, A review of the immune molecules in the sea cucumber, Fish Shellfish Immunol. 44 (2015) 1–11. https://doi.org/10.1016/j.fsi.2015.01.026.
[17] T. Hibino, M. Loza-Coll, C. Messier, A.J. Majeske, A.H. Cohen, D.P. Terwilliger, K.M. Buckley, V. Brockton, S.V. Nair, K. Berney, S.D. Fugmann, M.K. Anderson, Z. Pancer, R.A. Cameron, L.C. Smith, J.P. Rast, The immune gene repertoire encoded in the purple sea urchin genome, Dev. Biol. 300 (2006) 349–365. https://doi.org/10.1016/j.ydbio.2006.08.065.
[18] L. Terrana, I. Eeckhaut, Taxonomic description and 3D modelling of a new species of myzostomid (Annelida, Myzostomida) associated with black corals from Madagascar, Zootaxa 4244 (2017). https://doi.org/10.11646/zootaxa.4244.2.9.
[19] F.S. Chia, J. Xing, Echinoderm coelomocytes, Zool. Stud. 35 (1996) 231–254.
[20] Q. Li, R. rong Qi, Y. nan Wang, S. gen Ye, G. Qiao, H. Li, Comparison of cells free in coelomic and water-vascular system of sea cucumber, *Apostichopus japonicus*, Fish Shellfish Immunol. 35 (2013) 1654–1657. https://doi.org/10.1016/j.fsi.2013.07.020.
[21] C. Canicatti, G. D'Ancona, E. Farina- Lipari, The coelomocytes of *Holothuria polii* (Echinodermata). I. light and electron microscopy, Bolletino Zool. 56 (1989) 29–36. https://doi.org/10.1080/11250008909355618.
[22] V. Queiroz, M. Mauro, V. Arizza, M.R. Custódio, M. Vazzana, The use of an integrative approach to identify coelomocytes in three species of the genus *Holothuria* (Echinodermata), Invertebr. Biol. 141 (2022). https://doi.org/10.1111/ivb.12357.
[23] G. Caulier, S. Jobson, N. Wambreuse, L. Borrello, J. Delroisse, I. Eeckhaut, A. Mercier, J.-F. Hamel, Vibratile cells and hemocytes in sea cucumbers—Clarifications and new paradigms, in: World Sea Cucumbers, Elsevier, 2024: pp. 403–412. https://doi.org/10.1016/B978-0-323-95377-1.00024-2.
[24] Q. Li, Y. Ren, L. Luan, J. Zhang, G. Qiao, Y. Wang, S. Ye, R. Li, Localization and characterization of hematopoietic tissues in adult sea cucumber, *Apostichopus japonicus*, Fish Shellfish Immunol. 84 (2019) 1–7. https://doi.org/10.1016/j.fsi.2018.09.058.
[25] I.M. Dubovskiy, N.A. Kryukova, V.V. Glupov, N.A. Ratcliffe, Encapsulation and nodulation in insects, Invertebr. Surviv. J. (2016) 229-246 Pages. https://doi.org/10.25431/1824-307X/ISJ.V13I1.229-246.

[26] S. Jobson, J.-F. Hamel, A. Mercier, Rainbow bodies: Revisiting the diversity of coelomocyte aggregates and their synthesis in echinoderms, Fish Shellfish Immunol. 122 (2022) 352–365. https://doi.org/10.1016/j.fsi.2022.02.009.
[27] V. Matranga, G. Toia, R. Bonaventura, W.E.G. Müller, Cellular and biochemical responses to environmental and experimentally induced stress in sea urchin coelomocytes, Cell Stress Chaperones. 5 (2000) 113. https://doi.org/10.1379/1466-1268(2000)005<0113:CABRTE>2.0.CO;2.
[28] J. Hamel, J. Sun, B.L. Gianasi, E.M. Montgomery, E.L. Kenchington, B. Burel, S. Rowe, P.D. Winger, A. Mercier, Active buoyancy adjustment increases dispersal potential in benthic marine animals, J. Anim. Ecol. 88 (2019) 820–832. https://doi.org/10.1111/1365-2656.12943.
[29] X. Wu, T. Chen, D. Huo, Z. Yu, Y. Ruan, C. Cheng, X. Jiang, C. Ren, Transcriptomic analysis of sea cucumber (*Holothuria leucospilota*) coelomocytes revealed the echinoderm cytokine response during immune challenge, BMC Genomics. 21 (2020) 306. https://doi.org/10.1186/s12864-020-6698-6.
[30] M. Chiaramonte, R. Russo, The echinoderm innate humoral immune response, Ital. J. Zool. 82 (2015) 300–308. https://doi.org/10.1080/11250003.2015.1061615.
[31] T. Korn, E. Bettelli, M. Oukka, V.K. Kuchroo, IL-17 and Th17 Cells, Annu. Rev. Immunol. 27 (2009) 485–517. https://doi.org/10.1146/annurev.immunol.021908.132710.
[32] E. Meunier, P. Broz, Evolutionary Convergence and Divergence in NLR Function and Structure, Trends Immunol. 38 (2017) 744–757. https://doi.org/10.1016/j.it.2017.04.005.
[33] L.X. Li, X.H. Liu, H. Wang, L. Wang, B. Han, Y.Q. Chang, J. Ding, Molecular characterization and expression of NLRP10 in the antibacterial host defense of the sea cucumber (*Apostichopus japonicus*), Gene. 675 (2018) 110–118. https://doi.org/10.1016/j.gene.2018.06.072.
[34] Z. Lv, Z. Wei, Z. Zhang, C. Li, Y. Shao, W. Zhang, X. Zhao, Y. Li, X. Duan, J. Xiong, Characterization of NLRP3-like gene from *Apostichopus japonicus* provides new evidence on inflammation response in invertebrates, Fish Shellfish Immunol. 68 (2017) 114–123. https://doi.org/10.1016/j.fsi.2017.07.024.
[35] N.M. Gowda, U. Goswami, M. Islam Khan, T-antigen binding lectin with antibacterial activity from marine invertebrate, sea cucumber (*Holothuria scabra*): Possible involvement in differential recognition of bacteria, J. Invertebr. Pathol. 99 (2008) 141–145. https://doi.org/10.1016/j.jip.2008.04.003.
[36] X. Wei, X. Liu, J. Yang, S. Wang, G. Sun, J. Yang, Critical roles of sea cucumber C-type lectin in non-self recognition and bacterial clearance, Fish Shellfish Immunol. 45 (2015) 791–799. https://doi.org/10.1016/j.fsi.2015.05.037.
[37] J.S. Elenbaas, U. Pudupakkam, K.J. Ashworth, C.J. Kang, V. Patel, K. Santana, I.-H. Jung, P.C. Lee, K.H. Burks, J.M. Amrute, R.P. Mecham, C.M. Halabi, A. Alisio, J. Di Paola, N.O. Stitziel, SVEP1 is an endogenous ligand for the orphan receptor PEAR1, Nat. Commun. 14 (2023) 850. https://doi.org/10.1038/s41467-023-36486-0.
[38] L. Verstrepen, I. Carpentier, R. Beyaert, The Biology of A20-Binding Inhibitors of NF-κB Activation (ABINS), in: C. Ferran (Ed.), Mult. Ther. Targets A20, Springer New York, New York, NY, 2014: pp. 13–31. https://doi.org/10.1007/978-1-4939-0398-6_2.
[39] C. Xu, P. Zheng, S. Shen, Y. Xu, L. Wei, H. Gao, S. Wang, C. Zhu, Y. Tang, J. Wu, Q. Zhang, Y. Shi, NMR structure and regulated expression in APL cell of

human SH3BGRL3, FEBS Lett. 579 (2005) 2788–2794. https://doi.org/10.1016/j.febslet.2005.04.011.
[40] Y. Wang, J. Diao, B. Wang, X. Xu, M. Gui, C. Li, M. Guo, A second FADD mediates coelomocyte apoptosis response to *Vibrio splendidus* infection in sea cucumber *Apostichopus japonicus*, Fish Shellfish Immunol. 127 (2022) 396–404. https://doi.org/10.1016/j.fsi.2022.06.046.
[41] J.M. Rodriguez, M.A. Glozak, Y. Ma, W.D. Cress, Bok, Bcl-2-related Ovarian Killer, Is Cell Cycle-regulated and Sensitizes to Stress-induced Apoptosis, J. Biol. Chem. 281 (2006) 22729–22735. https://doi.org/10.1074/jbc.M604705200.
[42] B.J. Hillier, V.D. Vacquier, Amassin, an olfactomedin protein, mediates the massive intercellular adhesion of sea urchin coelomocytes, J. Cell Biol. 160 (2003) 597–604. https://doi.org/10.1083/jcb.200210053.
[43] L. D'Andrea-Winslow, D.W. Radke, T. Utecht, T. Kaneko, K. Akasaka, Sea urchin coelomocyte arylsulfatase: a modulator of the echinoderm clotting pathway, Integr. Zool. 7 (2012) 61–73. https://doi.org/10.1111/j.1749-4877.2011.00279.x.
[44] M.B. Ponczek, M.Z. Bijak, P.Z. Nowak, Evolution of Thrombin and Other Hemostatic Proteases by Survey of Protochordate, Hemichordate, and Echinoderm Genomes, J. Mol. Evol. 74 (2012) 319–331. https://doi.org/10.1007/s00239-012-9509-0.
[45] Z. Wang, C. Li, R. Xing, Y. Shao, X. Zhao, W. Zhang, M. Guo, β-Integrin mediates LPS-induced coelomocyte apoptosis in sea cucumber *Apostichopus japonicus* via the integrin/FAK/caspase-3 signaling pathway, Dev. Comp. Immunol. 91 (2019) 26–36. https://doi.org/10.1016/j.dci.2018.10.004.
[46] R.P.A. Wallin, A. Lundqvist, S.H. Moré, A. Von Bonin, R. Kiessling, H.-G. Ljunggren, Heat-shock proteins as activators of the innate immune system, Trends Immunol. 23 (2002) 130–135. https://doi.org/10.1016/S1471-4906(01)02168-8.
[47] H. Zhao, H. Yang, H. Zhao, M. Chen, T. Wang, The molecular characterization and expression of heat shock protein 90 (Hsp90) and 26 (Hsp26) cDNAs in sea cucumber (*Apostichopus japonicus*), Cell Stress Chaperones. 16 (2011) 481–493. https://doi.org/10.1007/s12192-011-0260-z.
[48] E.E. Battin, J.L. Brumaghim, Antioxidant Activity of Sulfur and Selenium: A Review of Reactive Oxygen Species Scavenging, Glutathione Peroxidase, and Metal-Binding Antioxidant Mechanisms, Cell Biochem. Biophys. 55 (2009) 1–23. https://doi.org/10.1007/s12013-009-9054-7.
[49] H. Ba, F. Yao, L. Yang, T. Qin, H. Luan, Z. Li, X. Zou, L. Hou, Identification and expression patterns of extracellular matrix-associated genes fibropellin-ia and tenascin involved in regeneration of sea cucumber *Apostichopus japonicus*, Gene. 565 (2015) 96–105. https://doi.org/10.1016/j.gene.2015.03.071.
[50] K. Mehta, U. Shahid, F. Malavasi, Human CD38, a cell-surface protein with multiple functions, FASEB J. 10 (1996) 1408–1417. https://doi.org/10.1096/fasebj.10.12.8903511.
[51] L. Cerenius, K. Söderhäll, Immune properties of invertebrate phenoloxidases, Dev. Comp. Immunol. 122 (2021) 104098. https://doi.org/10.1016/j.dci.2021.104098.
[52] J. Jiang, Z. Zhou, Y. Dong, H. Sun, Z. Chen, A. Yang, S. Gao, B. Wang, B. Jiang, X. Guan, Phenoloxidase from the sea cucumber *Apostichopus japonicus*: cDNA cloning, expression and substrate specificity analysis, Fish Shellfish Immunol. 36 (2014) 344–351. https://doi.org/10.1016/j.fsi.2013.12.001.

[53] Z. Wang, X. Fan, Z. Li, L. Guo, Y. Ren, Q. Li, Comparative analysis for immune response of coelomic fluid from coelom and polian vesicle in *Apostichopus japonicus* to *Vibrio splendidus* infection, Fish Shellfish Immunol. Rep. 4 (2023) 100074. https://doi.org/10.1016/j.fsirep.2022.100074.
[54] C. Liu, C. Yang, M. Wang, S. Jiang, Q. Yi, W. Wang, L. Wang, L. Song, A CD63 Homolog Specially Recruited to the Fungi-Contained Phagosomes Is Involved in the Cellular Immune Response of Oyster Crassostrea gigas, Front. Immunol. 11 (2020) 1379. https://doi.org/10.3389/fimmu.2020.01379.
[55] K. Yu, X. Zhao, Y. Xiang, C. Li, Phenotypic and functional characterization of two coelomocyte subsets in *Apostichopus japonicus*, Fish Shellfish Immunol. 132 (2023) 108453. https://doi.org/10.1016/j.fsi.2022.108453.
[56] M. Oren, B. Rosental, T.S. Hawley, G.-Y. Kim, J. Agronin, C.R. Reynolds, L. Grayfer, L.C. Smith, Individual Sea Urchin Coelomocytes Undergo Somatic Immune Gene Diversification, Front. Immunol. 10 (2019) 1298. https://doi.org/10.3389/fimmu.2019.01298.
[57] G. T. Wilkins, Using novel sequence assembly strategies to resolve the transformer gene family, Macquarie University, Doctoral Thesis, 2020.
[58] K. Chen, S. Zhang, Y. Shao, M. Guo, W. Zhang, C. Li, A unique NLRC4 receptor from echinoderms mediates Vibrio phagocytosis via rearrangement of the cytoskeleton and polymerization of F-actin, PLOS Pathog. 17 (2021) e1010145. https://doi.org/10.1371/journal.ppat.1010145.
[59] X.-J. Li, L. Yang, D. Li, Y.-T. Zhu, Q. Wang, W.-W. Li, Pathogen-Specific Binding Soluble Down Syndrome Cell Adhesion Molecule (Dscam) Regulates Phagocytosis via Membrane-Bound Dscam in Crab, Front. Immunol. 9 (2018) 801. https://doi.org/10.3389/fimmu.2018.00801.